2010

Extreme Ultraviolet Spectral Streak Camera

John Michael Szilagyi
University of Central Florida

EXTREME ULTRAVIOLET SPECTRAL STREAK CAMERA

by

JOHN MICHAEL SZILAGYI

B.S. University of Central Florida, 2007

A thesis submitted in partial fulfillment of the requirements

for the degree of Master of Science

in the School of Electrical Engineering and Computer Science

in the College of Engineering and Computer Science

at the University of Central Florida

Orlando, Florida

Fall Term

2010

ABSTRACT

The recent development of extreme ultraviolet (EUV) sources has increased the need for diagnostic tools, and has opened up a previously limited portion of the spectrum. With ultrafast laser systems and spectroscopy moving into shorter timescales and wavelengths, the need for nanosecond scale imaging of EUV is increasing. EUV's high absorption has limited the number of imaging options due to the many atomic resonances in this spectrum. Currently EUV is imaged with photodiodes and X-ray CCDs. However photodiodes are limited in that they can only resolve intensity with respect to time and X-ray CCDs are limited to temporal resolution in the microsecond range.

This work shows a novel approach to imaging EUV light over a nanosecond time scale, by using an EUV scintillator to convert EUV to visible light imaged by a conventional streak camera. A laser produced plasma, using a mass-limited tin based target, provided EUV light which was imaged by a grazing incidence flat field spectrometer onto a Ce:YAG scintillator. The EUV spectrum (5 nm-20 nm) provided by the spectrometer is filter by a zirconium filter and then converted by the scintillator to visible light (550 nm) which can then be imaged with conventional optics. Visible light was imaged by an electron image tube based streak camera. The streak camera converts the visible light image to an electron image using a photocathode, and sweeps the image across a recording medium. The streak camera also provides amplification and gating of the image by the means of a micro channel plate, within the image tube, to compensate for low EUV intensities. The system provides 42 ns streaked images of light with a

temporal resolution of 440 ps at a repetition rate of 1 Hz. Upon calibration the EUV streak camera developed in this work will be used in future EUV development.

To my family

ACKNOWLEDGMENTS

I would like to express my gratitude to Dr. Martin Richardson for the support and guidance, and motivation throughout my studies and research, and the opportunities that made this work possible. I also would like to thank my committee members Dr. Patrick LiKamWa and Dr Samuel Richie for their time and effort in reading this thesis and valuable advice.

During this research many people have contributed to this project. Special thanks to Dr. Matthieu Baudelet for his valuable insights and ideas. I would also like to thank Mark Ramme, Reuvani Kamtaprasad, Omar Rodriguez, and Nathan Bodnar for their assistance in the laboratory and for the long hours spent revising my thesis. Thanks to Richard Zotti for all his help in the machine shop and assistance in the construction of this project. Also thanks to all the members of the Laser Plasma Laboratory for advice, assistance, and contribution to my work.

I finally would like to thank my family, without your support and motivation this important step in my life would not be possible.

TABLE OF CONTENTS

LIST OF FIGURES

LIST OF TABLES

LIST OF ACRONYMS

AMD - Acetone Methanol Deionized Water

CCD - Charge-Coupled Device

Ce:YAG - Cerium(III)-Doped Yttrium Aluminum Garnet

CMOS - Complementary Metal Oxide Semiconductor

EUV - Extreme Ultraviolet

EUVL - Extreme Ultraviolet Lithography

FFS - Flat Field Spectrometer

GPO - General Purpose Output

MCP - Micro-Channel Plate

MVC - Machine Vision Connector

PC - Photocathode

TTL - Transistor-Transistor Logic

UV - Ultra Violet

VMOS - Vertical Metal Oxide Semiconductor

CHAPTER 1: INTRODUCTION

Extreme ultraviolet (EUV) radiation is the spectral band between x-rays (5 nm or 250 eV) and ultraviolet (40 nm or 30 eV) [1]. Development of sources and applications for EUV has been a challenge due to the properties of light in this spectral region. At many atomic resonances, this band has high absorption in many materials (with complete absorption lengths shorter than 1 μm) and it is therefore, challenging to develop technologies utilizing EUV. EUV research has been limited to solar imaging of the sun's atmosphere. However over the last decade, EUV research has accelerated due to the need for shorter wavelength of light for imaging and lithography. With the development of EUV sources the need for diagnostic tools has increased [2]. Specifically, EUV generation necessitates the constant monitoring of the spectral intensity of the source to tune and maximize the desired wavelengths. A critical need for these measurements is in the development of plasma based sources for Extreme Ultra-Violet Lithography (EUVL). Understanding how plasma is formed and what atomic and molecular processes have an effect on the formation and absorption of EUV will help to optimize EUV intensities and wavelengths. One way of understanding the processes, such as the ionization stage and the electronic transitions in the plasma, is to measure the spectrum as the plasma forms and dissipates. Due to the small timescale that these processes occur over (less than 1 ns), high speed imaging is necessary.

For time resolved diagnostics, the streak camera is well suited to take images over short periods of time (picoseconds). When coupled with a spectrometer, time-resolved EUV spectra can be obtained. The EUV Spectral Streak Camera acquires EUV light and provides a

continuous spectral graph over a short period of time. This allows a non-steady state description of the EUV source emission. The electronic streak camera using an image tube generates an electron image of an optical slit along one axis and deflects it over a recording medium along a perpendicular axis, so that time is resolved as a spatial dimension. Streak cameras are arguably one of the best devices for measuring the intensity of light with picosecond accuracy on a one shot basis [3]. In order to provide an EUV streaked spectrum, the output of a flat-field spectrometer (FFS) was imaged onto a thin Ce:YAG scintillator. The scintillator converted the ionizing radiation of the EUV to visible light, corresponding to the peak sensitivity of the streak cameras photocathode. This provides a robust solution for converting an EUV image to an electron image. This resulting image then can be swept by an electric field across a detector providing a streaked image over a short time scale.

Applications such as laser plasma source generation will benefit from the ability to characterize sub-nanosecond atomic processes producing EUV [4]. Being able to observe the spectrum in picosecond time scale will allow atomic processes to be determined, which leads to an improved efficiency in the generation of EUV source plasma. In spectroscopy of materials this camera would add to the spectrum available for identifying materials and composition. As more applications for EUV are developed, an effective means for measuring the wavelength and intensity over short periods of time will be vital. Using an EUV streak camera will satisfy this need, and will help develop EUV technology further.

CHAPTER 2: EXTREME ULTRAVIOLET

Extreme Ultraviolet (EUV) is the band of light between x-rays and ultraviolet, with a corresponding wavelength of 5 nm (250 eV) to 40 nm (30 eV) [1] as seen in Figure 2.1 [1].

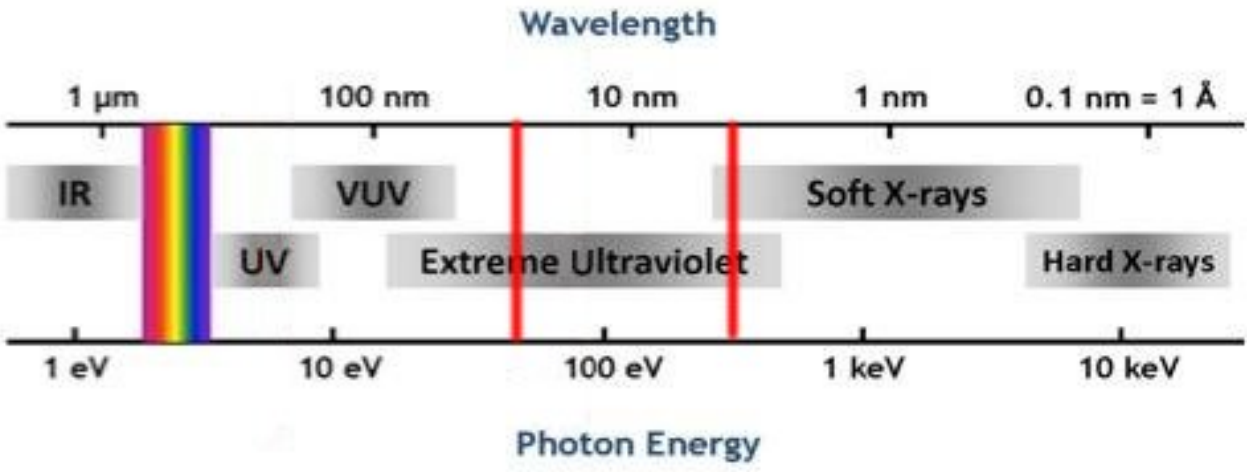

Figure 2.1: EUV band shown in relationship to the optical spectrum

EUV detectors have long been used by satellites to study solar phenomenon [5]. EUV's application, in the last decade, in lithography has expanded greatly due to the new field of Extreme Ultraviolet Lithography (EUVL). EUV is critical to the development of the next generation of semiconductor chip manufacture so that the International Technology Roadmap for Semiconductors [2] can be met. EUV's resonance with many low and intermediate Z (atomic number) elements makes the light readily absorbed by most materials. This absorption makes mirrors and imaging devices difficult to make, but also lends itself for sensing of low Z elements like carbon, nitrogen and oxygen with spectroscopy.

2.1 PROPERTIES

EUV has several properties that make it both useful and difficult to use. The most notable characteristic of EUV is its high absorption into many materials, with absorption lengths less than 1 μm. This is due to the many resonances with low and intermediate Z element's orbitals, providing the ability of using EUV for sensing low Z elements. These resonances come from the ability of EUV to strip the core electrons in the s1 and s2 orbitals [1]. For this reason EUV is difficult to work with because it is quickly absorbed in air and therefore must be used in vacuum. This also prevents standard optics such as lenses from being used and requires expensive multilayer and grazing incidence mirrors.

EUV's wavelength (5 nm-40 nm) is ideal for the next generation of lithography for semiconductor manufacturing due to its shorter wavelength than current processes [2]. Coupled with its high absorption, it is also useful for imaging biological structures in microscopy. The limiting factor of the imaging resolution is dictated by the Rayleigh criterion, defined by,

$$R = \frac{1.22 \cdot \lambda}{2NA}$$

where NA is the numerical aperture of the focusing element, λ is the wavelength of incident radiation, and R is the minimum resolvable feature size in meters. This puts a range of resolution well into the tens of nanometers.

Another notable property of EUV is that it is an ionizing radiation, where its energy is sufficient to strip the electrons away from atoms thereby ionizing them. This has an effect of

stripping the atoms from materials that EUV is incident on. This makes developing imaging surfaces for EUV difficult to use because they will degrade with time. Ionizing radiation also has the ability to create charges in materials which can create currents and charges that can damage detectors.

2.2 APPLICATIONS

Like other bands of light, EUV has many uses across a wide variety of fields. Some of these uses are solar imaging, spectroscopy, microscopy, and EUV Lithography. In solar imaging 17.1, 19.5, 28.4, and 30.4 nanometer wavelengths are imaged, corresponding to 0.07, 1, 1.5, and 2 million degrees Kelvin respectively. Hotter plasmas exist higher in altitude in the suns atmosphere the plasma being imaged occurs [5]. This allows for mapping of thermal and magnetic dynamics in the suns atmosphere.

With EUV spectroscopy ion transitions in high energy plasmas can be determined. This allows for identification of materials involved in the plasma and to develop new EUV sources [6]. EUV used in microscopy allows for nano-scale imaging with higher resolution than that of longer wavelengths. The lower photon energies compared to X-ray imaging allows for biological samples to be imaged over longer periods of time with reduced damage to the samples [7].

One of the more prevalent uses for EUV has been for the EUV Lithography (EUVL). Lithography is the used to produce microprocessors, and to keep pace with Moore's law EUV has been determined to be the next light source [2]. In EUVL EUV is often produced by a

plasma source and is then focused to expose the photo resist ink on the silicon for etching. By using EUV, in lithograph, smaller feature sizes are possible than with UV. EUVL has predominately used 13.5 nm light due to the current multilayer mirrors having high reflectivity centered at this wavelength.

The EUV source used to characterize and setup this project was a mass limited Sn-doped laser pumped plasma source [8]. This source was developed by CREOL in the University of Central Florida for the EUVL source development program. It uses a stream of tin doped droplets, 30 μm in diameter, that are dispensed at a rate of 10-100 kHz. These droplets are then targeted by a 1064 nm pulsed laser that ionizes the droplets to produce a plasma that emits EUV at 13.5 nm. This EUV source was used because it can produced metered amounts of EUV light at defined intervals. This provides a known source to characterize the EUV streak camera.

2.3 IMAGING

2.3.1 Current Technology

Several X-ray CCD cameras have been a used for many years to image EUV sources, and to record EUV spectra. They typically have 6-10 micron pixel size and can have a response time in the millisecond range. [9] CCDs must be exposed directly to vacuum to allow EUV to reach the CCD. These devices provide a reliable method for capturing spatial and temporal information about and EUV source or an object illuminated by EUV.

Another common technology used in EUV imaging is EUV photodiodes. These are similar to other photodiodes but due to EUV's high absorption, the depletion zone of the junction must be close to the surface and the electrode cannot cover the diode. The response time of EUV photodiodes had been shown to fall in the hundreds of nanoseconds, and is good for measuring the intensity of EUV sources. [10]

To direct EUV light to detectors and targets multilayer mirrors have to be used. These mirrors are produced by depositing layers (40-50) of high Z and low Z materials using precision vapor deposition. [11] These mirrors use interference and Bragg scattering to redirect the EUV light. The Bragg scattering is defined as follows,

$$m \cdot \lambda = 2 \cdot \mathrm{d} \cdot \sin\theta \sqrt{1 - \frac{4 \cdot \delta^2}{m^2 \lambda^2}}$$

where d is the layer periodicity, m is the diffraction order, δ is the bilayer weighted real part of the refractive index, and θ is the angle between the incident ray and the scattering ray. [1] This principle is shown in Figure 2.2. For EUV these layers are typically made of molybdenum and silicon or molybdenum and beryllium. The molybdenum layer is thicker providing scattering and the lower Z layer (silicon or beryllium) with its lower absorption provides spacing of the molybdenum, as seen in Figure 2.2.

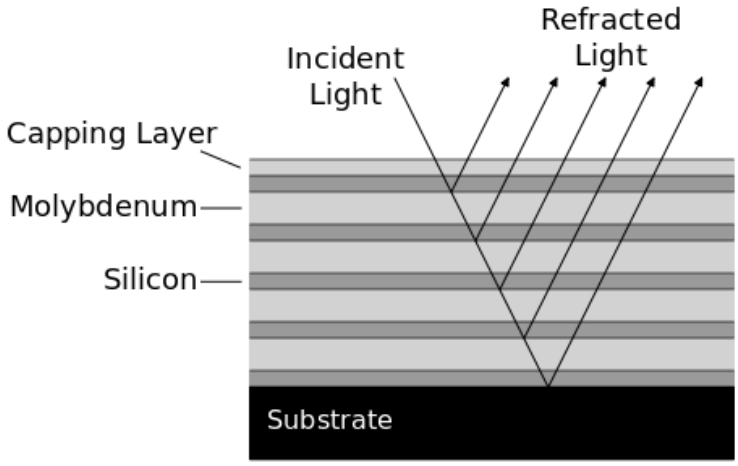

Figure 2.2: Multilayer mirror scattering incident light and showing layer structure

These multilayer mirrors typically have approximately 70% maximum reflection (normal to surface) in a narrow range (typically less than 1 nm) in the EUV band, and their peak wavelengths can be adjusted by adjusting the periodicity of the layers. [12]

2.3.2 Temporal Imaging

To record temporal information, CCD cameras, photodiodes, and streak cameras can be used. CCDs are the devices, providing millisecond temporal resolution. To record faster events photodiodes can be used, providing nanosecond resolution. Photodiodes are a good alternative to CCDs for temporal measurements due to their size and cost. Streak cameras are good for capturing events in the sub-nanosecond range or shorter. The streak camera creates an electron image which is then swept across a phosphor, which creates an image with the temporal

information stored in the spatial domain. This allows conventional devices such as CCDs to record the faster events.

2.3.3 Spectral Imaging

In order to image spectral information of EUV, EUV photodiodes and CCD spectrometers are most often used. EUV photodiodes with band-pass optical filters provide the intensity measurement of a narrow band of EUV light. The filters used are typically made of thin layers (less than 1 μm) of low Z materials. In order to record the intensity of multiple wavelengths of light simultaneously, several photodiodes with different types of filters need to be used.

In order to resolve a more complete spectral image than an individual photodiode a spectrometer is used. One method of mapping the spectrum intensity of an EUV source is to scan a photodiode across the spectrum provided by a diffraction grating, which then provides an electric signal that corresponds to the spectral intensity [13]. This, however, cannot provide a spectral intensity map for short events due to the scanning time of the photodiode. To capture the spectrum of an EUV source, a CCD camera is combined with the spectrometer to record the intensity for multiple wavelengths. This can provide a spectrum of EUV for an event in the tens of milliseconds [9]. In this project an electron image tube streak camera, discussed in Chapter 3, is used to image the spectrum of EUV provided by a grating. The image of the grating is converted to an electron image and swept across the output of the streak camera's phosphor

where it is converted to visible light. This image is then captured by a visible light CCD camera, allowing for spectral information to be captured over very short periods of time.

2.4 SPECTROMETER

To obtain spectral information about EUV, a flat-field grazing incident spectrometer was used to separate the wavelength content of the incident light. With the high absorption of EUV a grazing incidence grating is advantageous to improve reflectivity [14]. To improve the spectral resolution across the incoming bandwidth from 5 nm to 20 nm, the grating uses a variable groove configuration with average grove spacing of 1095-1450 lines per mm with a nominal spacing of 1200 lines per mm. The spectrometer is based on the Rowland circle configuration that is common to many spectrometers. An entrance slit placed on the circle projecting light on to the grating will project the corresponding spectrum onto the surface of the circle. Due to the curvature of the circle the grating has a radius of curvature to compensate the curve projection. The compensation provides a flat field projection of the spectrum which is ideal for the flat surface of the streak camera. [15] With the blaze angle of 3 degrees the incident light will be at an angle of 87 degrees from the normal of the grating as seen in Figure 2.3 [16]. Using the grating equation shown below, the range of output angles can be found for the grating.

$$m \cdot \lambda = \sigma_0[\sin\alpha + \sin\beta]$$

Where m is the order of diffraction, λ is the wavelength in meters, σ_0 is the nominal grove spacing in meters, α is the incident angle, and β is the output angle [14].

Due to the small size of the scintillating crystal the streak camera must be placed closer to the grating than the ideal distance. This has an effect of blurring the spectrum and therefore the spectral resolution. Another option is to shift the streak camera across the spectrum at the ideal distance, but this would limit the range of wavelengths seen by the camera at a given time.

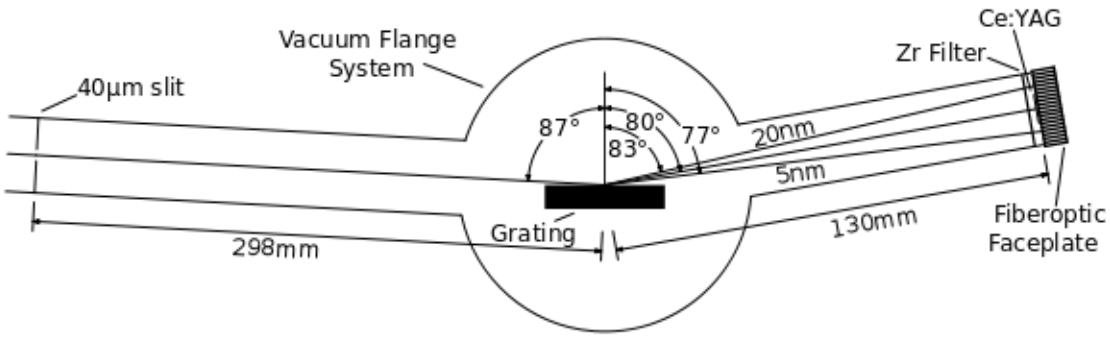

Figure 2.3: Properties of the Hitachi 001-0266 grating and spectrometer

CHAPTER 3: STREAK CAMERA

3.1 PRINCIPLES

The streak camera is an imaging device that takes a 1-dimensional spatial image of incident light and streaks it across a recording medium in the second spatial domain. This records the time domain in a spatial domain at very high speeds, providing for a light intensity vs. time image over a very short time period as seen in Figure 3.1. Streak cameras typically are one of two types: mechanical, using rotating mirrors to sweep an optical image across the recording medium, or an electronic streak camera, using an image tube and an electric charge to sweep an electron image across a recording medium. Mechanical streak cameras are limited in the maximum speed at which they can rotate their mirror. This inherently limits the time resolution to microseconds. An electron image tube however can reach time resolutions in the femtosecond range [17]. For this project a picosecond time resolution was required, and therefore an image tube streak camera was used.

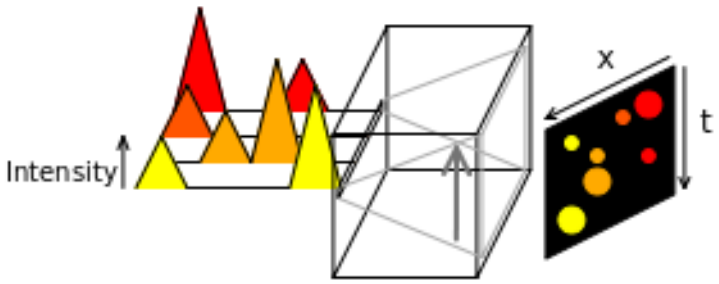

Figure 3.1: Principles of streak camera operation

3.1.1 Principles of Streak Camera Operation

An image tube streak camera converts incoming photons of an optical image and converts it to an electron image by means of a photoluminescent photocathode. The resulting electrons are accelerated toward an anode through an electric field, which also focuses the electrons on the phosphor. A varying electric field deflects the electron image across a phosphor. The phosphor then converts the electrons to photons corresponding to the streaked image which can then be recorded by an optical device. In the project a micro channel plate is located between the deflecting field and the phosphor in order to amplify the intensity of the electron image.

3.2 IMAGE TUBE

The image tube in the streak camera used in this project is manufactured by Kentech Instruments, LTD, as part of the OSC12 line of streak cameras. It is a 1st generation; micro channel plate gated and intensified streak tube. The tube uses an S-20 photocathode (Na_2KSb:Cs), and a P-20 phosphor ((Zn,Cd)S:Ag). The photocathode gives the image tube a peak sensitivity at 475 nm and the phosphor provides output at 560 nm.

3.2.1 Physical Description

The image tube (Figure 3.2) is housed in the OSC12 camera body. Its compact body is 15 cm ± 0.5 cm long (dependent on manufacturing), along its optical axis allowing for easy installation in measurement applications. The tube is enclosed in an aluminum enclosure that

allows for mounting external devices. Inside the enclosure the image tube is filled with high voltage potting to protect the tubes envelope, and to prevent the bias and streak voltage from arcing or leaking from the tube.

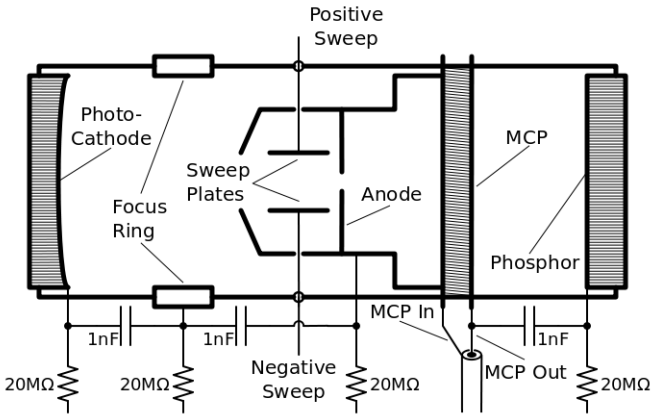

Figure 3.2: Internal layout of the image tube [18]

Internally the image tube consists of a fiber optic faceplate coated with a photocathode, followed by the focus ring. They are followed by the cathode aperture, the sweep deflection plates, and the anode aperture. Behind the anode aperture is a micro-channel plate (MCP) followed by the phosphor coated on the output fiber optic plate. Several bias resistors and capacitors are encased in potting in order to keep them as close to the image tube as possible. This and several high voltage wires passing through the potting make up the image tube.

3.2.2 Photocathode

The photocathode in this streak camera is made of S-20 photoemissive multi-alkali material (Na_2KSb:Cs) coated on the concave vacuum side of the input fiber optic plate. This

absorbs the incoming photons into the material and excites the valence electron to the ionization state with a maximum emission energy E_{em} of,

$$E_{em} = E_p - (E_A + E_G)$$

where, $E_p = hc/\lambda$ is the energy of an incoming photon, E_A is the electron affinity, and E_G is the forbidden band [17]. The electrons are then transferred through the film of the photocathode to the opposite surface of the film, and then escape into the vacuum where an electrostatic potential of -5.2 kV accelerates the electrons into the image tube vacuum. There are several losses associated with this process, such as absorption, transport, and surface barrier losses, which decrease the efficiency of the photocathode. Losses are due to imperfect band absorption, reflections, and transmissions through the photocathode. Reflection losses are reduced by 1/4 wave antireflective coatings on the photocathode. Transmission losses are reduced by increasing the thickness of the photocathode, but with diminishing effectiveness. As the thickness of the photocathode reaches 120 nm, collision losses start reducing the efficiency. [17] These are common to S20 photocathodes and can be reduced by monitoring the sensitivity of the photocathode during production [19].

Transport losses are caused by electron crystal lattice collisions, and phonon production due to lattice scattering. Many of the produced electrons will lose less than 0.01 eV per collision event which can render them with insufficient energy to contribute to photo emission and will be reabsorbed [17].

Surface barrier losses are caused by surface electrostatic forces which prevent electrons with energies below 0.3 eV to 0.4 eV from leaving the semiconductor. This effectively limits the upper range of spectral sensitivity of the photocathode to 850 nm as seen in Figure 3.3 [20]. Surface barrier losses account for the majority of losses in the photocathode.

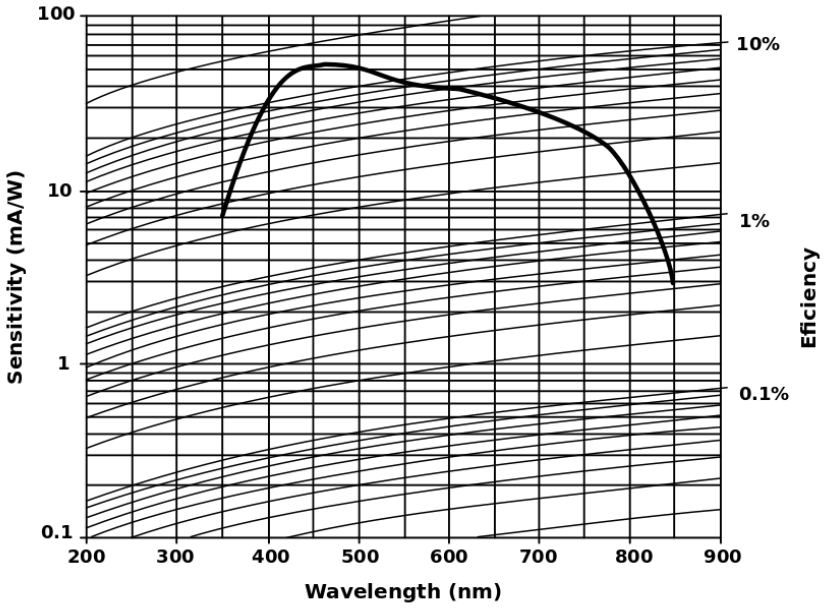

Figure 3.3: Spectral response of S-20 photocathodes

The S-20 photocathode is made of Na_2KSb:Cs. This photocathode is made by depositing a layer of Na_2KSb on the faceplate. Then a layer of Cesium is deposited on top of the primary layer to reduce the surface affinity of the photocathode. S-20 has a peak sensitivity of 78 mA/W at approximately 475 nm, with sensitivity across the 350 nm-850 nm range. The peak efficiency of this photocathode is around 30% in the UV range, 10% in the red range, and 1% in the infrared range. [17]

3.2.3 Focus

Once the electrons leave the photocathode they are accelerated by an electrostatic field where, like a lens, they converge at the edge of the anode cone, and then diverge until they reach the micro channel plate creating an inverted image. The focusing is performed by the shape of the anode cone and the focusing ring. The focus plates maintain a potential of 3.5 kV adjustable ± 0.1 kV, relative to the photocathode voltage. This allows the adjustment of the focus of the image on the MCP.

3.2.4 Deflection

After the electrons have passed the aperture of the anode cone, they are deflected by the sweep deflection plates from the negative to the positive. The sweep deflection plates accomplish this by applying a 1.5 kV potential to the left plate and a -1.5 kV the right plate and them ramping the potential to 0 kV. This deflects the electrons across the micro channel plate (MCP), effectively sweeping the image over the MCP. The temporal resolution of the streak camera is dependent on the speed of this ram function. To sweep over a very short period of time the voltage on the plates must be of sufficient voltage to deflect the electron image completely.

3.2.5 Micro Channel Plate

The micro channel plate (MCP) is used to amplify the electron signal. The MCP is made up of a 2 mm sheet of silicon oxide with an array of closely packed 6 μm diameter micro tubes

that go through the MCP at an angle approximately 8 degrees. Each face of the MCP is coated in a conductive layer with the input side at the anode potential and the output side at negative potential with respect to the anode. As seen in Figure 3.4, the MCP in this project has a potential of -1.35 kV across it.

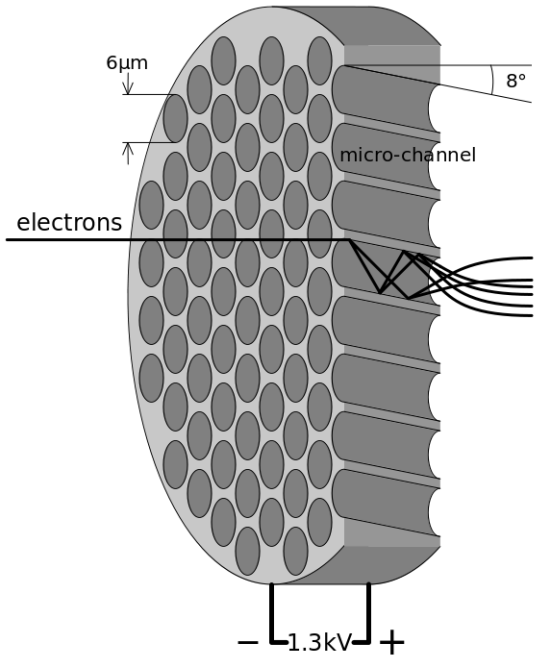

Figure 3.4: Micro channel plate with electron being multiplied

When an electron enters one of the micro tubes it hits the side of the tube and dislodges another electron from the medium, due to the potential across the tube. More electrons become extracted with each impact until it reaches the output of the MCP. There the resulting stream of electrons is accelerated toward the phosphor by the voltage differential. In the image tube the MCP acts as a gate when the potential across the MCP is 0 kV with a response time of approximately 10 ns. By varying the voltage across the MCP the level of amplification can be changed.

3.2.6 Phosphor

A phosphor in the streak camera converts the amplified electrons from the MCP into photons. The phosphor is made of a film of aluminum followed by a layer of $(Zn, Cd)S: Ag$ on the output fiber optic faceplate. $(Zn, Cd)S: Ag$ is a mixture of ZnS and CdS crystals which is activated by silver and co-activated by chlorine. As seen in Figure 3.5 [17], when an electron hits the crystal lattice, free electrons and holes are generated, after losing energy to phonon generation, the holes are trapped by the activators and the electrons are trapped in unoccupied energy levels. Then by thermal agitation the electrons recombine with the trapped holes at the activators emitting photons.

Losses through this process are due to electrons recombining through non radiative transitions, losses due to the aluminum film, material absorption of produced photons, and phonon generation. However the largest losses are due to the initial electron/hole pair generation and phonon generations. The efficiency of the phosphor is about .1 depending on electron beam voltage relative to the phosphor. The light output of the phosphor is a yellow-green ranging from 450 nm to 750 nm with a peak at 560 nm (Figure 3.6) [17]. The average decay time of the brightness to 10% is about 0.2 ms which is sufficient for a CCD CAMERA to be able to record the image and limits the maximum rep rate of the streak camera.

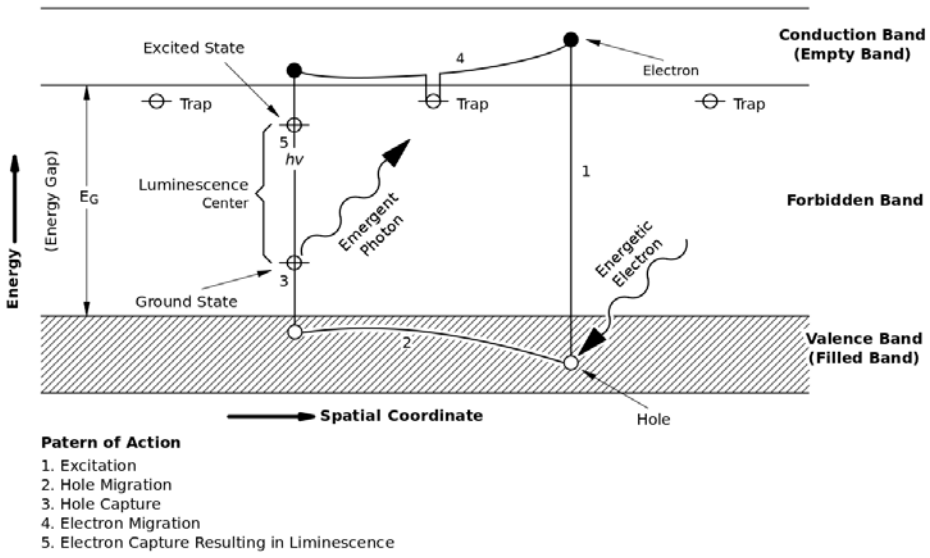

Figure 3.5: Process of luminescence for phosphor

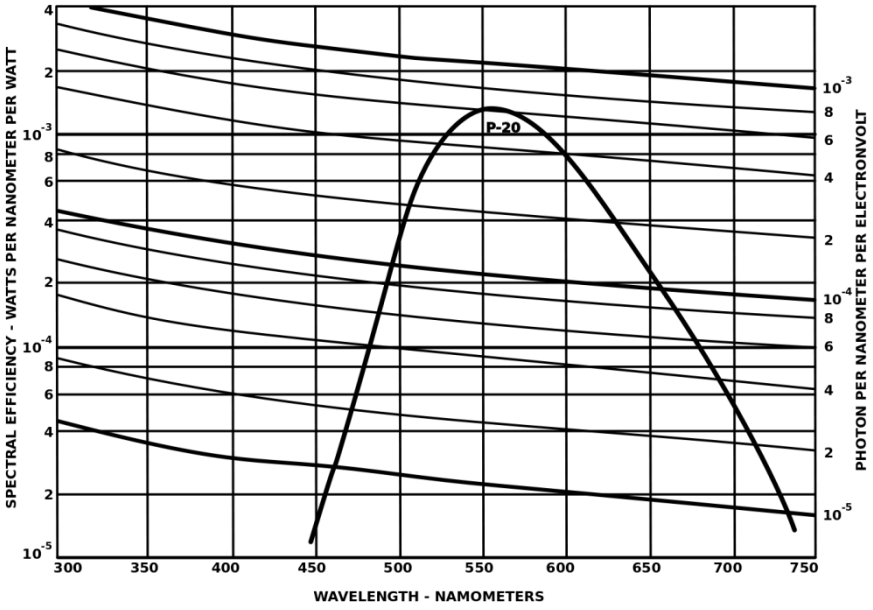

Figure 3.6: Spectral emission characteristics of phosphor P-20

3.2.7 Optical Properties

The image tube of the streak camera in many ways is like an optical lens system except that the imaged is resolved with electrons. One significant difference is that the image tube has a gain function that allows the light amplification to be varied proportionally with voltage. When no voltage is present across the MCP the image is not reproduced providing a gating function.

3.2.7.1 Gain

Positive gain of the image tube is due to the combined effects of the MCP and the phosphor. While the MCP contributes to the highest intensity gain of the image, the phosphor also increases the signal. This gain is necessary to compensate for the losses incurred by scattering and phonon absorption in the photocathode, reflection in the fiber optic faceplates, and reflections of the aluminum coating on the phosphor. By varying the voltage across the MCP the gain of the streak camera can be adjusted.

3.2.7.2 Temporal and Spatial Resolution

The temporal resolution of the streak camera is limited to,

$$\tau = \frac{1}{R\nu}$$

where R is the spatial resolution of the image, and ν is the streak velocity in mm/s [17]. The temporal resolution was measured by measuring the size of the spot produced by an

instantaneous event at a known repetition rate. The repetition rate was produced by a Spectra Physics Spitfire Ti:Sapphire 100 femtosecond laser at a repetition rate of 1 kHz. In order for the laser to fall in the spectral range of the of the streak camera, the pulse was up-converted to 400 nm. The laser output was directed through a 67 cm long, multi-pass cavity, with a HR mirror and a 90% output coupler. This produced a 5 pulse burst, with pulses separated by 4.47 ns at a 1 kHz rep rate as seen in Figure 3.7.

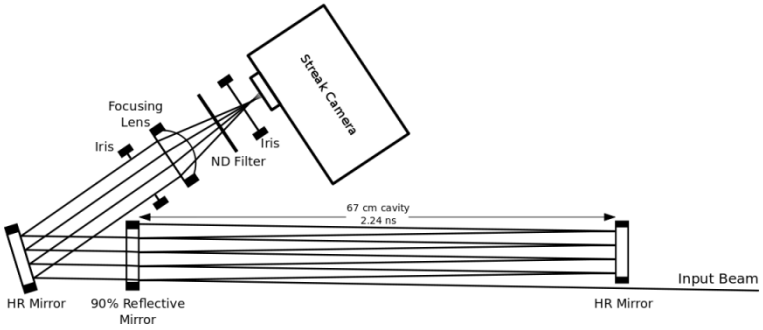

Figure 3.7: Diagram of the mirror pulse delay cavity

With the streak camera synchronized to capture one group of 5 pulses every 1 second, and the gain of the image tube set to a minimum to prevent distortion, the following streaked image (Figure 3.8) of the pulses where obtained.

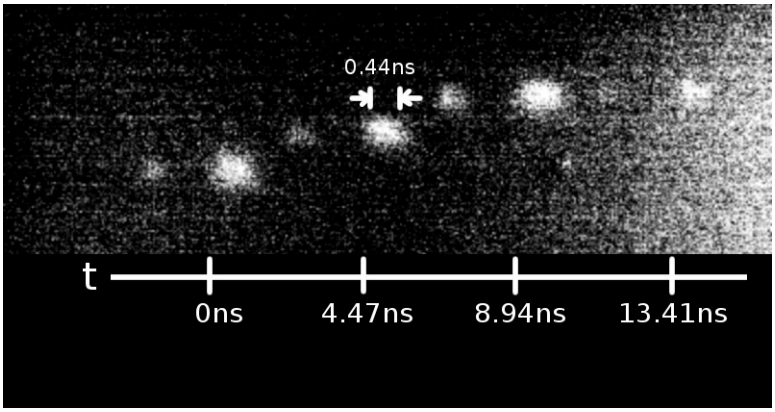

Figure 3.8: Streak image of the 4 pulses

By measuring the FWHM ($w_{pulse\ width}$) of the imaged pulses (in pixels), and dividing that value by the spacing ($w_{pulse\ separation}$) of the imaged pulses (in pixels), the time ratio was determined. When the time ratio is multiplied by pulse separation (t_{period}=4.47 ns), the minimum temporal resolution (t_{min}) is determined to be 440 ps.

$$t_{min} = \frac{w_{pulse\ width}}{w_{pulse\ separation}} \cdot t_{period}$$

This result is the minimum length event that the image tube can resolve without loss of data. The 440 ps resolution is due to the delay in photocathode response and propagation of the electrons in the image tube. In order for the camera to reach its temporal resolution, the minimum resolvable spatial detail should be larger than the minimum time step on the streaked image.

The spatial resolution of the image tube was determined by placing a USAF 1951 resolution chart directly in contact with the input fiber optic faceplate, which was illuminated with a uniform light source. The gain of the image tube was adjusted to a minimum to prevent distortion and the MCP was set to “DC” on mode. A high resolution CCD camera was fitted with

a 10x microscope objective to record the image (Figure 3.9) without significantly affecting the resolution.

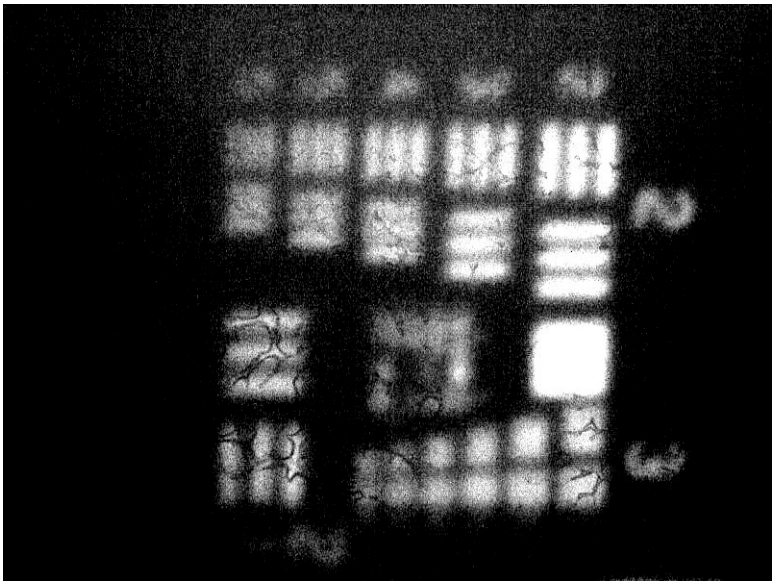

Figure 3.9: USAF 1951 Resolution chart image through the streak camera image tube with 10x objective and CCD camera

The minimum resolution is where the contrast transfer function (CTF) is 3% at a defined spatial frequency. The CTF is defined by the following equation.

$$CTF = (B_{max} - B_{min})/(B_{max} + B_{min})$$

where, B_{max} is the maximum luminance value, and B_{min} is the minimum luminance value [17]. Using image processing software to quantify the image, the values for the equation where obtained and a spatial resolution of 54.3 line pairs/mm was determined.

3.3 ELECTRONICS

Within the streak camera, most of the electronics where designed and manufactured by Kentech Instruments, LTD. In addition to these electronics external trigger and timing circuits were added to control the sweep, MCP, and CCD timing of the camera with respect to the input light source.

3.3.1 Description/Block Diagram

The streak camera electronics are separated into several discrete circuits. This allows for easy modification of the streak camera properties since any circuit can be replaced to change the parameters of the streak camera. Below in Figure 3.10 is a block diagram of the streak camera electronics.

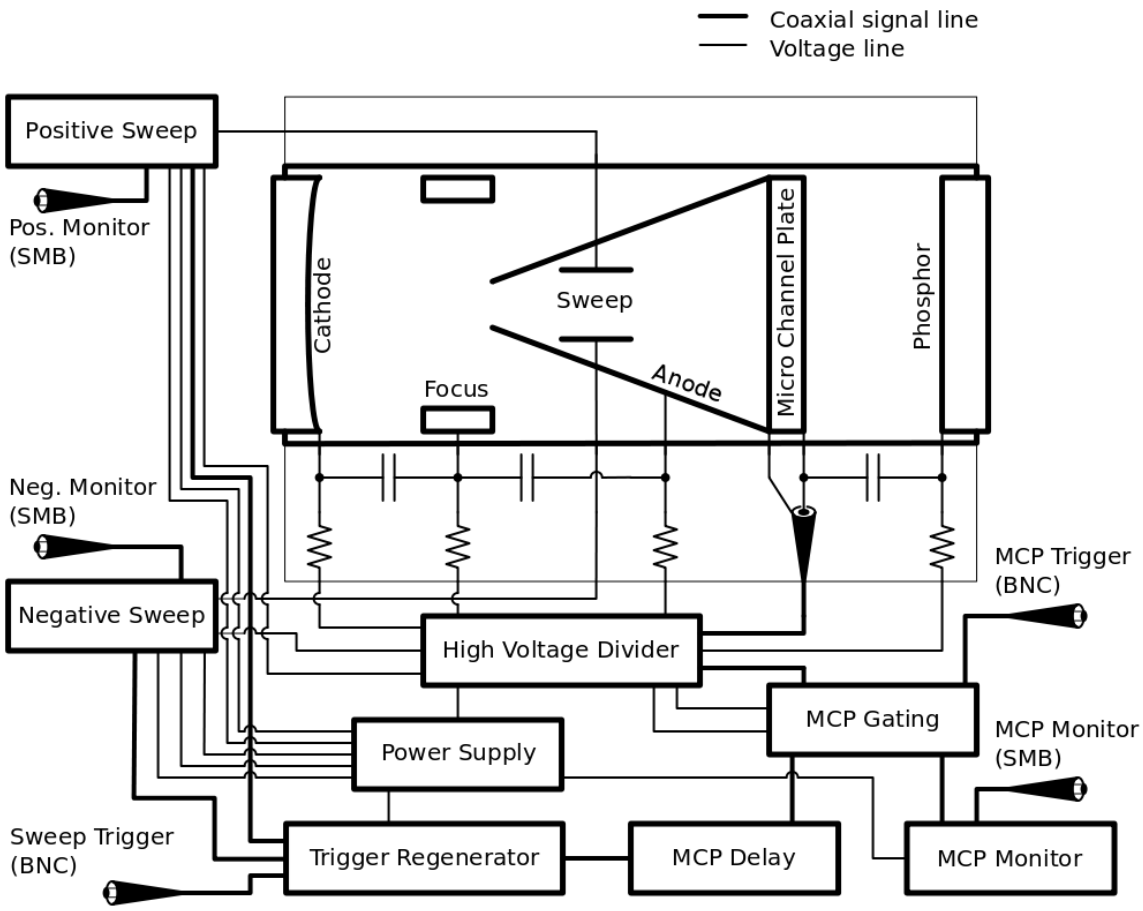

Figure 3.10: Block Diagram of Electronics

The Power Supply provides several voltages to different circuits listed below.

- +20 V
  - Trigger Regenerator
  - Sweep
  - Negative Sweep
  - MCP Monitor
- -20 V
  - Negative Sweep
- +9.5 kV

    - Voltage Divider
- -1.5 kV
    - Positive Sweep
- +1.5 kV
    - Negative Sweep

Following the sweep trigger pulse signal the Trigger Regenerator has a Sweep Trigger input and sends out a regenerated signal to the Positive Sweep, Negative Sweep, and MCP Delay. The MCP Delay delays the signal by 8 to 28 nanoseconds via a rotary switch. From there the signal is passed to the MCP Gating circuit to turn off the MCP. The gating circuit has an input for turning on the MCP with an output to the MCP Monitor which in turn outputs a monitor signal for the MCP. From the MCP Gating circuit the high voltage MCP on/off signal enters the High Voltage Divider where the voltage can be adjusted to change the gain of the MCP. This high voltage signal then goes to the MCP in the image tube. The High Voltage Divider provides several voltages for the image tube and other circuits. It provides the voltages to operate the image tube. It also provides an adjustable bias for the Positive and Negative Sweep, and power for the MCP Gating circuit. The voltages provided the image tube elements are show in Table 3.1 below.

Table 3.1: Voltage provided to image tube elements

Voltage (kV)	Image tube element
-9.5	Cathode
-9.12 to -8.87&Focus	-9.12 to -8.87&Focus
-5.64 to -4.31	negative bias for Positive Sweep
-4.29	Anode
-4.27 to -2.94	positive bias for Negative Sweep
-3.78 to -3.80	MCP
0 and +1.5	Phosphor

3.3.2 Power Supply

The power supply is divided into two sections as seen in Figure 3.11. The first section is a +20 V and -20 V power supply regulated by a LM317 and LM337 respectively. These supply up to 1.5 A to the Micro Channel Plate (MCP) Monitor circuit, the Positive and Negative Sweep circuit, and the Trigger Regenerator circuit. The second part of the power supply is the high voltage portion of the power supply. This portion is powered by a +20 V power supply regulated by a LM338. This regulates power to a 9.5 kV supply, a 1.5 kV and a 1.5 kV supplies, regulated each by a LM317. The power supply also has the energizing coils for relays RL1 and RL2 which are triggered by switch S3. These relays bypass power to the MCP and Phosphor of the image tube so that a non-streaked image can be obtained.

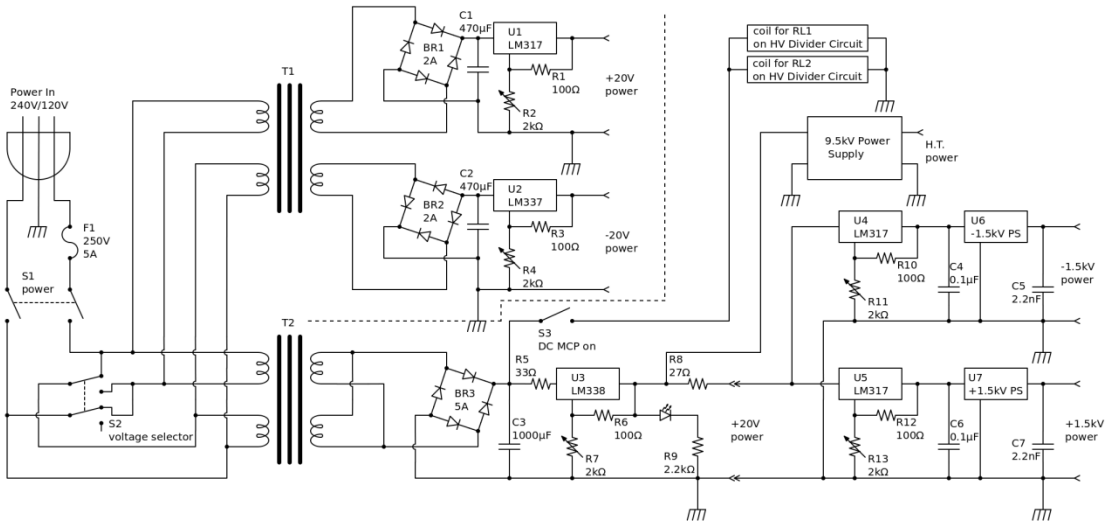

Figure 3.11: Power Supply Circuit

3.3.3 High Voltage Divider Circuit

The image tube of the streak camera needs several stable voltages to form the electron lens and to gate the micro channel plate (MCP). These voltages are set by the High Voltage Divider circuit by dividing 9.5 kV form the power supply. In addition this circuit also provides adjustment for the gain of the MCP, the bias for the Positive and Negative Sweep circuits, and adjusts the focus voltage.

The resistor divider adjusts the voltage on the focus plates relative to the cathode in order to focus the electron lens onto the MCP. This is accomplished by R1-R3 by a simple resistive voltage divider. The Focus voltage range is 376 V to 627 V with respect to the Cathode voltage of -9.5 kV. The remaining -3.86 kV is divided by Zener diodes Z1-Z22 as seen in Figure 3.12. Z1-Z5 divides the voltage down to -2.51 kV which is sent to the anode of the image tube, the

input face of the MCP, and as -VE to the MCP Gating circuit. Z6-Z10 divides the voltage down to -1.16 kV for +VE of the MCP Gating circuit. The remaining Zener diodes Z11-Z22 regulate the voltage down to ground.

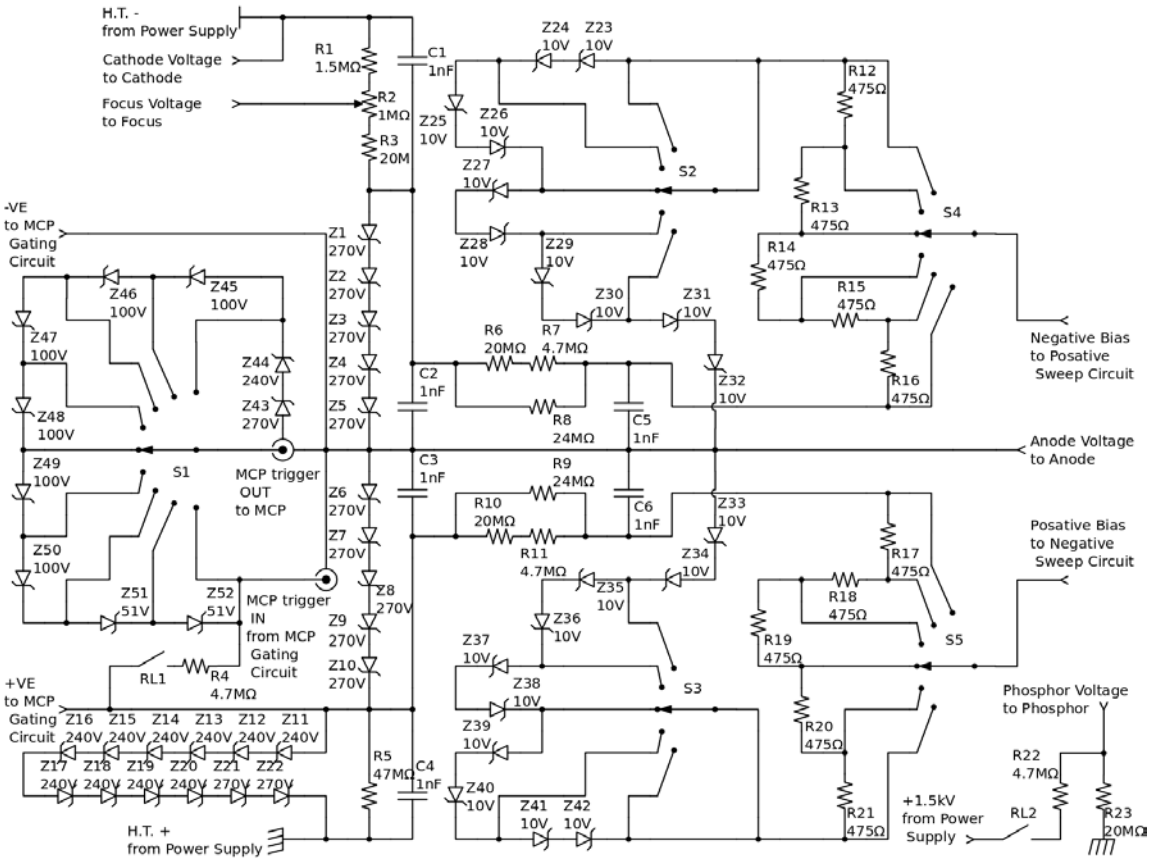

Figure 3.12: High Voltage Divider Circuit

To shift the electron image on the MCP, the bias voltage is adjusted on the sweep plates. This is accomplished by a symmetric voltage divider network with a coarse and fine adjustment for the voltage. The divider provides a voltage of positive 20 V to 1350 V for the Negative Sweep circuit, and negative 20 V to 1350 V for the Positive Sweep circuit each with 30 steps. The course adjustment is provided by Zener diodes Z23-Z42 and external rotary switch S2-S3.

Fine adjustment of the voltage is provide by the resistor network made of resistors R12-R21 and rotary switch S4-S5 as seen in Figure 3.12.

Gain of the MCP is set by a divider network made up of Zener diodes Z43-Z52, and rotary switch S1 (Figure 3.12) which divides either the input pulse or the DC signal. When the MCP is active the divider network can set the applied voltage across the MCP from 510 V to 1350 V in 9 steps, increasing or decreasing gain.

The MCP divider network can be bypassed by relay RL1 which sends DC voltage to the MCP turning it on. In addition relay RL2 connects the phosphor to the +1.5 kV power supply. Together these relays provide a static, non-streaked image on the phosphor. These relays are activated by an external button S3 on the power supply.

3.3.4 Sweep Generating Circuit

In order to sweep the electron image across the MCP a positive and negative high voltage ramp needs to be placed on the deflection plates. This is accomplished by two separate sweep ramp generators: a positive sweep and a negative sweep generator. The sweep boards are comprised of 3 sections. The first section is the input trigger filter and amplifier. This section rectifies and filters the input signal with C1-C2, R1-R2, and D1 as seen later in Figure 3.13 and Figure 3.14. This signal is then amplified with a common emitter circuit triggering common collector circuit using R3-R6, and Q1 and Q2. This output signal is then passed to the second part of the circuit, an avalanche Miller integrator. The Miller integrator integrates the resulting

signal and inverts the signal to form a linear high voltage ramp on the sweep plates. This ramp function is biased through R21 from the High Voltage Divider circuit. In order to adjust the ramp time capacitor C6 is adjusted to control the time constant of the Miller integrator. The third and final section of the circuit is the sweep monitor. This monitor outputs a square wave pulse for the duration of the ramp signal and the circuit reset time (≈3 ms). This part of the circuit allows the high voltage sweep to be monitored in order to adjust the timing of the sweep plates with respect to each other and to the MCP.

3.3.4.1 Positive Sweep

The Positive Sweep circuit, as seen later in Figure 3.13, is supplied by the +20 V and -1500 V from the power supply. The -1500 volts is ramped to ground resulting in a capacitor C11 producing a positive pulse on the output of 40 ns. This output is biased with -20 V to -1350 V from the High Voltage Divider circuit through R21. The monitor circuit in the Positive Sweep circuit held to 5.6 V by Z11 until the Q6 pulls the output to 0 V when the ramp circuit is active.

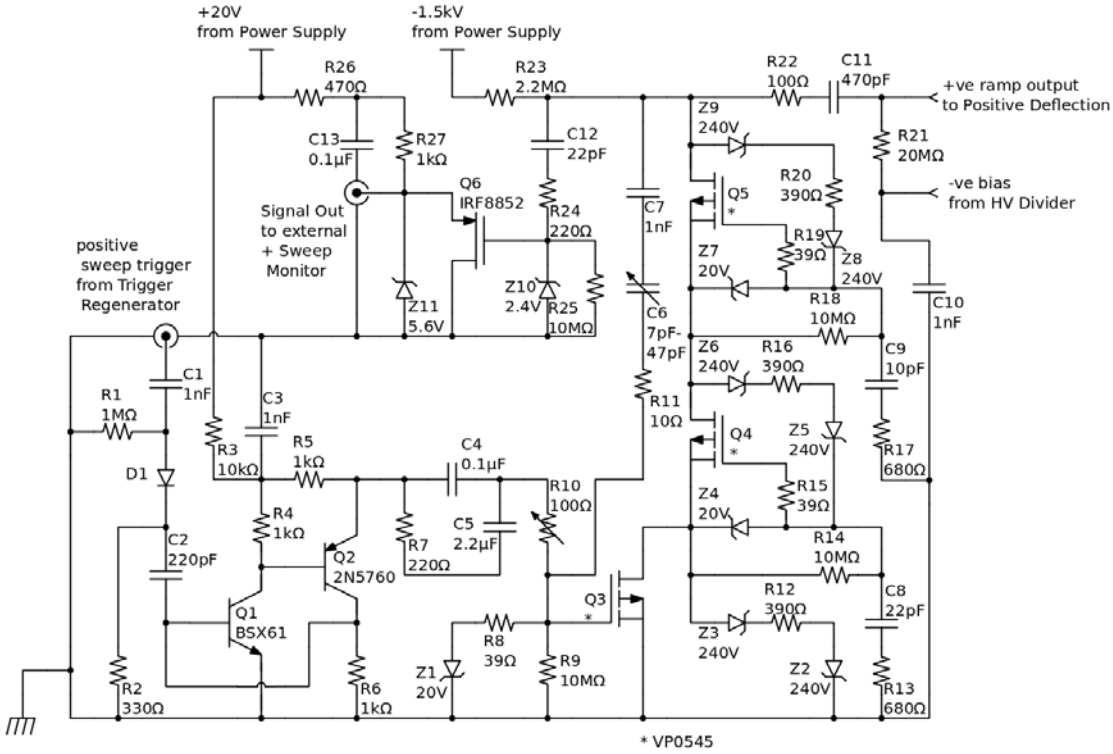

Figure 3.13: Positive Sweep Circuit

3.3.4.2 Negative Sweep

The Negative Sweep circuit, as seen later in Figure 3.14, is supplied by the +20 V, -20 V, and +1500 V from the power supply. The +1500 V is ramped to ground resulting in a capacitor C11 producing a negative pulse on the output of 40 ns. This output is biased with +20 V to +1350 V from the High Voltage Divider circuit through R21. The monitor circuit in the Positive Sweep circuit is supplied by the -20 V power supply but is held to 5.6 V by Z11 and the +20 V power supply. When the ramp circuit is active, Q6 pulls the output to 0 V.

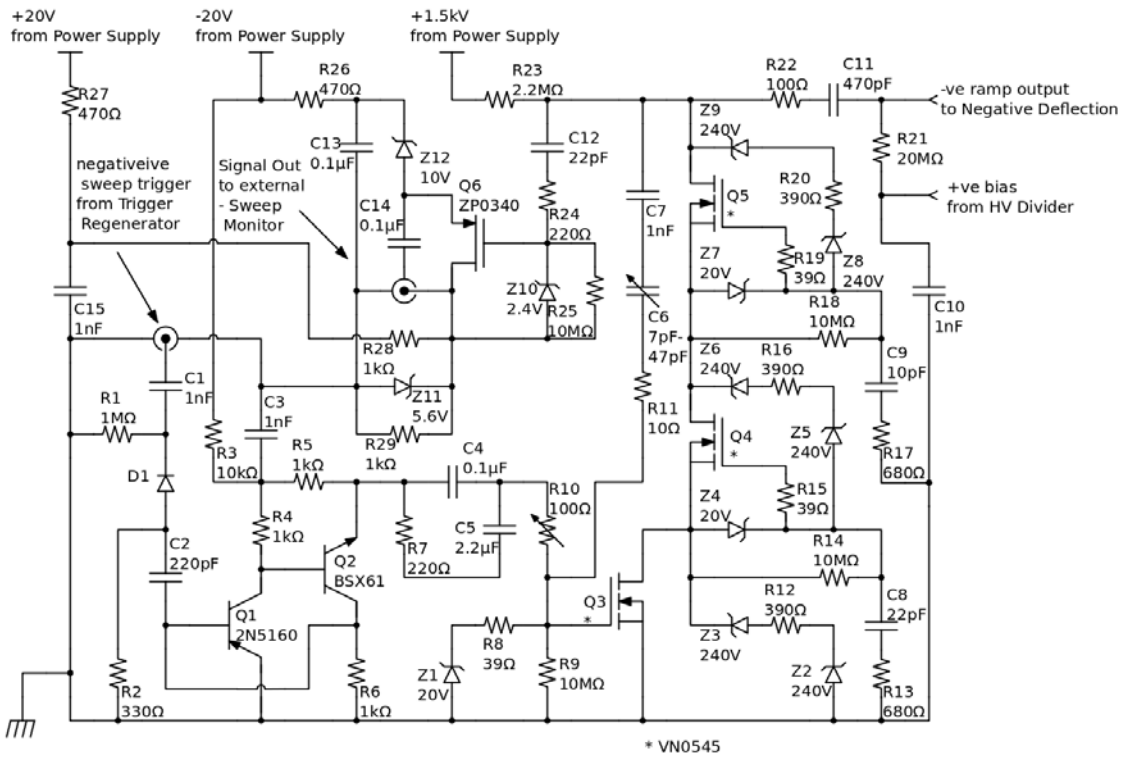

Figure 3.14: Negative Sweep Circuit

3.3.5 MCP Gating Circuit

The MCP Gating circuit monitors several signals and turns on or off the MCP and provides a monitor of the MCP. The circuit provides the gating voltage, provided to the High Voltage Divider circuit for gating the MCP. The circuit is comprised of 3 sections, the MCP on trigger, MCP off trigger, and MCP monitor as seen in Figure 3.15.

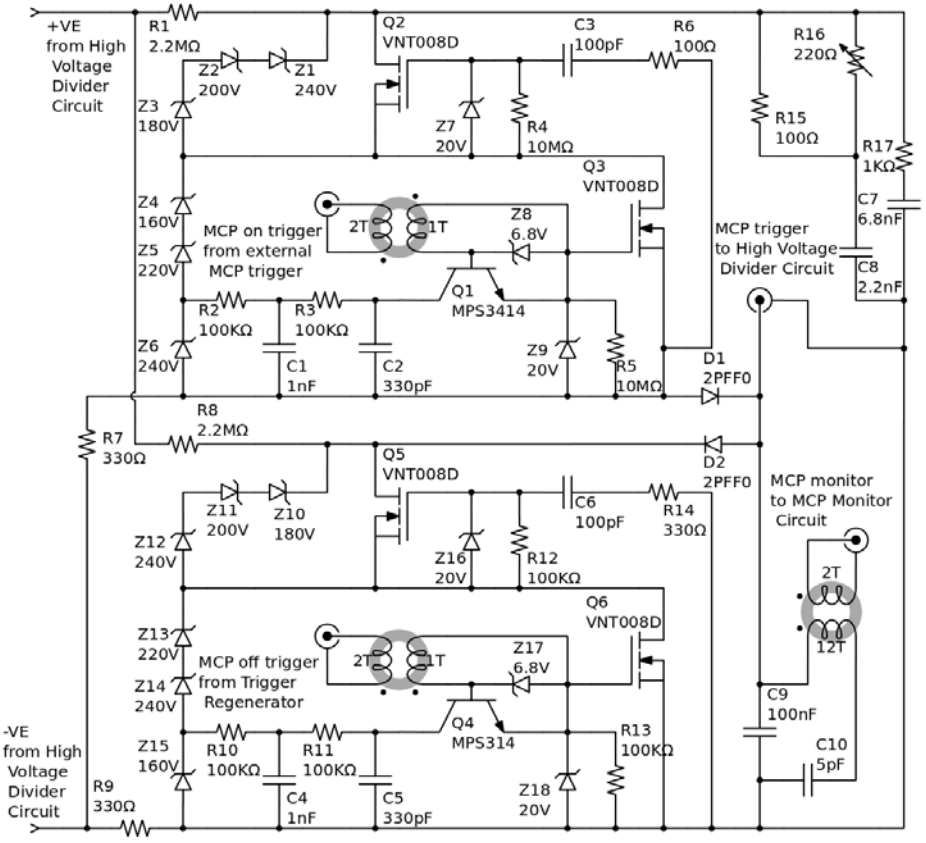

Figure 3.15: MCP Gating Circuit

The MCP on trigger network is triggered by an external source through a 2:1 signal transformer. This signal is then clipped to 6.8 V by Zener diode Z8 to turn on the Q1 in a common emitter configuration. This in turn triggers an avalanche circuit comprised of Q2-Q3, Z7, Z9, R4-R6, and C3. The voltages supplied to this portion of the circuit are regulated by Zener diodes Z1-Z6. In order to adjust the turn on response of the circuit R15-R16, and C8 form an adjustable (R16) filter network to prevent triggering on spurious signals.

The MCP off trigger portion of the circuit is identical to the MCP on portion, except that it is configured to pull the output voltage from -1.16 kV to -2.51 kV. This portion of the circuit

also resets the MCP on trigger portion of the circuit. The input of this circuit is triggered by the trigger regenerator circuit through a 2:1 signal transformer.

The MCP monitor trigger portion of the circuit is coupled to the signal output through a 6:1 transformer and capacitor C10 in series. This provides an output pulse amplitude of 5 V.

3.3.6 Trigger Regenerator Circuit

The Trigger Regenerator circuit is needed to synchronize the Positive and Negative Sweep circuits and the MCP off trigger with a long input trigger [18]. The input signal of this circuit is a 10 V signal terminated into a 50 Ω load. The input pulse is shortened with C2-C3 and R2-R3 and rectified with D1 (Figure 3.16) to a 200 ns pulse. This pulse triggers a common emitter NPN bipolar transistor, which in turn triggers a common collector PNP transistor which sinks current of the output transformer. The outputs of the transformer trigger, the Positive and Negative Sweep circuits, and the MCP circuit.

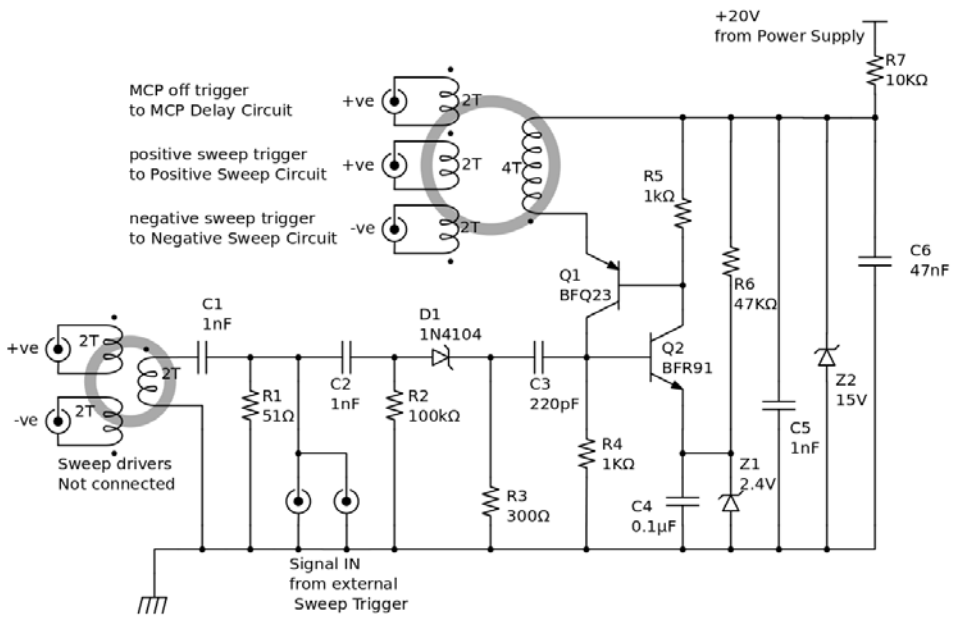

Figure 3.16: Trigger Regenerator Circuit

3.3.6.1 MCP Delay Circuit

Through the MCP Delay circuit, a delay of 8 to 28 ns with 1 ns steps (adjustable via rotary switch) is added to the Trigger Regenerator circuit signal. This delayed signal is then sent to the MCP Gating circuit off trigger. This circuit, as seen in Figure 3.17, allows for the end of the gating to be adjusted close to the end of the camera's image sweep, therefore preventing the bright after image. The circuit is made up of 3 delay ICs with 1 ns steps, and a 21 position switch to select the amount of delay. The output for this circuit is 50 Ω, provided for by R1 in Figure 3.17.

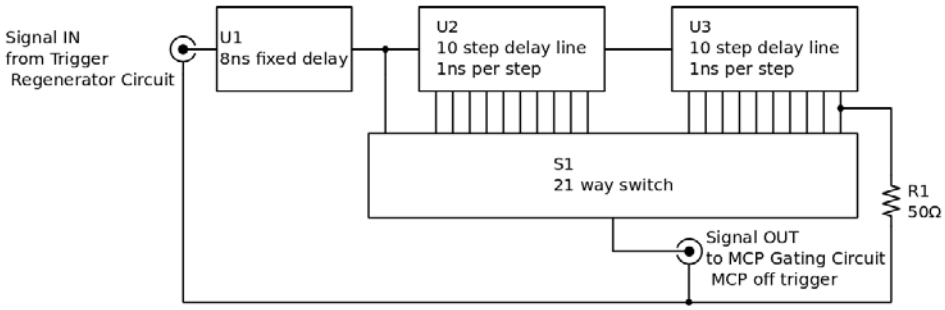

Figure 3.17: MCP off delay circuit

3.3.7 MCP Monitor Circuit

The MCP Monitoring circuit is a 5 V TTL level monitor of the voltage controlling the MCP. This circuit is supplied by the +20 V power supply feeding a LM7805 voltage regulator as seen in Figure 3.18, to provide 5 V for the TTL output. The input signal is connected through a SMB coaxial connection to the output signal transformer on the MCP Gating circuit Figure 3.18. The signal from the gating circuit triggers a Silicon Controlled Rectifier (SCR) through a voltage divider with Zener diode (R1 through R3, GA301, and Z1 in Figure 3.18). The SCR turns on and off a series of common emitter amplifiers (R4-R8, C1-C3, Q1, Q2 as seen in Figure 3.18) to render a TTL pulse. This is connected to an external TTL MCP monitor connector through a SMB coaxial connection.

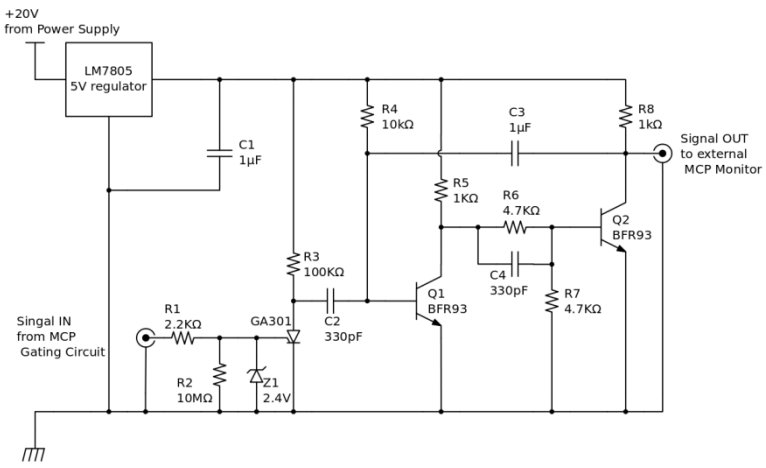

Figure 3.18: 5 V TTL level MCP monitor circuit

3.3.8 CCD

To record the image produced by the image tube a CCD camera is required. The used CCD camera for this project was a PixeLINK PL-A741 monochrome machine vision camera, as seen in Figure 3.19 [21].

Figure 3.19: PixeLINK PL-A741 camera

This camera was chosen for its small pixel size, and its versatility in triggering and image acquisition. Its spectral range is from 400 nm to 1000 nm, as seen in Figure 3.20 [21], which is sufficient to capture the 530 nm light emitted by the P-20 phosphor of the streak camera. The camera has a linear dynamic range of 60 dB with adjustable contrast points allowing for a dynamic range greater than 100 dB.

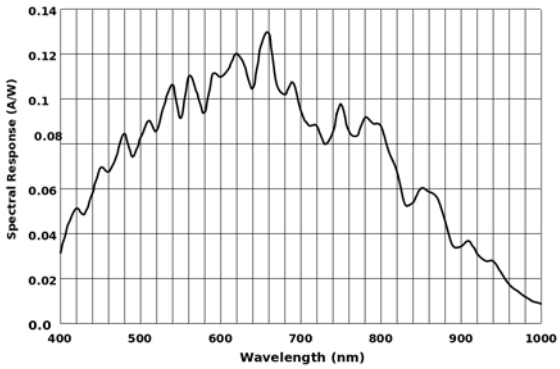

Figure 3.20: PL-A741 spectral response

3.3.8.1 Resolution

The PL-A741 is equipped with a 2/3 inch CCD with a resolution of 1280 x 1024 (8.57 mm x 6.912 mm, 11.01 mm diagonal),with 6.7 µm square pixels, and a pixel pitch of 6.7 µm x 6.75 µm [21]. Using the Modulation Transfer Function (MTF), shown below, the maximum resolution of the CCD can be calculated for each axis.

$$MTF_{\xi} = \left|\mathrm{sinc}\left(\pi \cdot x_{pitch} \cdot \xi\right) \cdot \sin(\pi \cdot x_{width} \cdot \xi)\right|$$

where ξ, x_{pitch}, x_{width} is the horizontal spatial frequency, pixel pitch, and pixel width respectively, and

$$MTF_{\eta} = \left|\mathrm{sinc}\left(\pi \cdot y_{pitch} \cdot \eta\right) \cdot \sin(\pi \cdot y_{width} \cdot \eta)\right|$$

where η, y_{pitch}, y_{width} is the vertical spatial frequency, pixel pitch, and pixel width respectively. [22] At a 3% MTF the maximum resolution is 253 line pairs per mm for the horizontal resolution and 248 line pairs per mm for the vertical resolution.

3.3.8.2 Interface and Control

The PL-A741 includes an IEEE 1394 interface for high speed (400 Mb/s) image transfer and an isolated programmable trigger. The camera is controlled through the IEEE port with the included software from PixeLINK. The CCD camera is triggered through a BNC adapter (provided by PixeLINK) which is connected to the timing system.

3.4 TIMING

For proper operation of the streak camera the precise timing of input light and the electronics is critical. Due to the recovery time of the phosphor and the streak electronics recharge time, the streak camera has a maximum cycle of one streak per second (1Hz). This timing is broken up into two categories, optical and electronic timing.

3.4.1 Electronic Timing

The timing of the electronics of the streak camera is controlled externally by a delay generator (Stanford Research Systems DG535). For a successful streak image capture, the MCP and the sweep circuit in the streak camera must be triggered with nanosecond accuracy from the light falling incident on the streak camera as seen in Figure 3.21 [18]). For the purposes of this project $T_0 = 0$ will be clock of the delay generator. At $T_0 = 0$ the MCP is triggered and after 23 ns turns on. The MCP will stay active for 7.88 ms or until it is turned off by the sweep off trigger. The sweep trigger must be triggered within 5-555 ns of the MCP trigger. Late sweep triggers will cause miss timings in the circuit. The image tube will start the sweep 42 ns after the sweep trigger, and will sweep the image across the phosphor for 31 ns. The streak circuit will then turn off the MCP. To capture the streaked image correctly the CCD must start integrating at the beginning of the sweep. The camera will continue integrating for the remainder of the cycle and will stop 5 ms before the next MCP trigger. This allows the CCD to capture more photons due to the persistence of the phosphor.

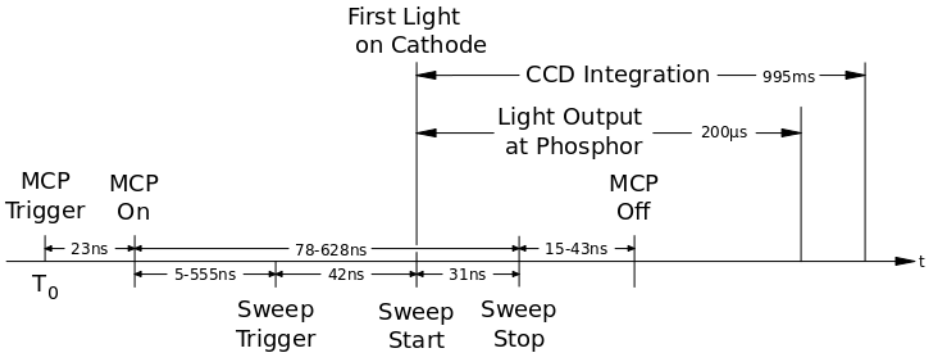

Figure 3.21: Streak camera timing diagram

3.4.2 Optical Timing

Light incident on the streak camera takes a predefined time to convert to an electron image, travel to the anode, and then convert to visible light. The first part of this timing is the conversion of the input light incident on the photocathode to an electron image. This timing is dependent on the emission time constant of the S-20 photocathode, and the delay caused by photon scattering within the photocathode. The electrons from the photocathode then take a set time to accelerate toward the anode. This time is defined by the voltage gradient between the photocathode and the output phosphor [17]

Once the electrons reach the phosphor there is a fixed time delay as the electron is absorbed by the P-20 phosphor and converted to photons. The radiative lifetime is the most significant factor in this delay. The most critical optical time constant is the persistence of the phosphor, which is the time that it takes for the phosphor to stop emission after electron absorption. [17] The emission time constant of the photocathode (1 ps) and the electron transit time (≈3 ns) are several orders of magnitude smaller than the delay caused by the phosphor persistence (1 ms) and can be ignored due to the delay generator in the streak camera. The total time from first incident light on the photocathode to the end of light output at the phosphor is approximately 1 ms as seen in Figure 3.21.

3.5 SOFTWARE

The software used for the streak camera is the PixeLINK Capture OEM provided with the PL-A741 CCD camera. This software provides CCD image capture adjustment as well as control of the external trigger functions. In this project the main functions used to control the CCD camera were the external shutter control, and the image capture functions. In addition, the software allows for the settings to be saved in firmware on the CCD camera so that the camera can remember predefined settings. The gain for the CCD camera was set to 9 dB to compensate for losses incurred in the streak camera. The camera has several predefined modes of operation that define how it reacts to eternal input. The external shutter control was set to trigger Mode 1. For the purpose of this project Mode 1 starts CCD integration on the falling edge of the external trigger and stops integration on the rising edge. Image capture was saved as lossless .TIFF to preserve the spectral and temporal resolution of the captured image.

CHAPTER 4: Ce:YAG

Cerium(III)-doped yttrium aluminum garnet, also known as Ce:YAG or P-46 phosphor, is a fast scintillator that emits a small flash of light when struck with ionizing radiation. These crystals are grown by the Czochralski method and then cut into thin slices for the use in scintillation. A Ce:YAG crystal (Figure 4.1) is used in this project to convert the EUV image into a visible light image that can be captured by the streak camera.

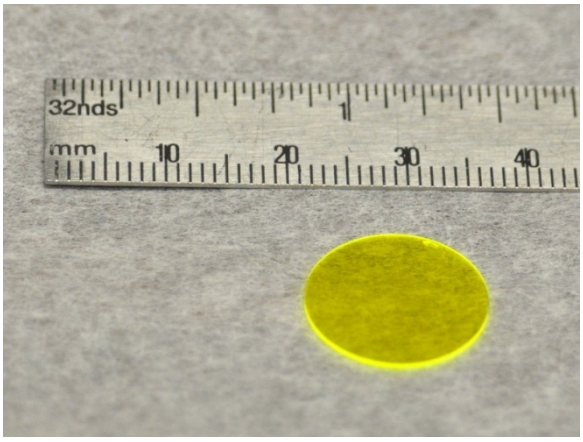

Figure 4.1: Ce:YAG crystal

4.1 PROPERTIES

4.1.1 Physical Properties

The crystal used in this project is 15 mm in diameter and 0.45 mm thick. This crystal is a single crystal with one of its cubic lattice faces parallel to the face of the crystal. The crystal orientation is important to maximize light penetration and conversion. The dimension of the

crystal matches closely to the maximum area image by the CCD through the streak camera, while providing perimeter space for mounting the crystal. Ce:YAG is a very durable crystal with a density of 4.55 g/cm^2 and a hardness of 8.5 Mohs [23]. This allows for simpler mounting techniques, and for the use of the crystal in harsher environments.

4.1.2 Chemical Properties

Ce:YAG is a synthetic yttrium aluminum garnet with a chemical formula of $Ce^{3+}:Y_3Al_5O_{12}$. This crystal is grown using the Czochralski method, which involves melting of the component materials and pulling a single crystal boule of Ce:YAG with the help of a seed crystal. [24] The crystal YAG used in this project is doped with Cerium at 0.2% with the cerium atoms replacing the yttrium atoms in the crystal lattice. While this doping is not the highest available, it is the most commercially available form of Ce:YAG. The lattice has cubic structure with a lattice constant of 12.01 angstrom that is aligned to the face of the crystal [23].

4.1.3 Absorption Properties

Optical absorption into the Ce:YAG crystal is due to transitions from the 4f ground state to the 5d states, and from the valence band to the conduction band. These transitions are at 178 nm, 230 nm, 340 nm and 450 nm respectively as seen in Figure 4.2 [25], [26].

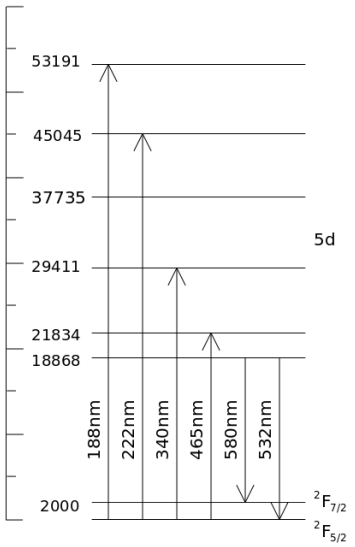

Figure 4.2: Ce:YAG emission and absorption band diagram

This yields an absorption spectrum with the highest peak at 450 nm as seen in Figure 4.3 [25]. In the case of EUV most of the absorption occurs from the valence band to the conduction band. The absorption coefficient for Ce:YAG is 0.074 mm^{-1} [27]

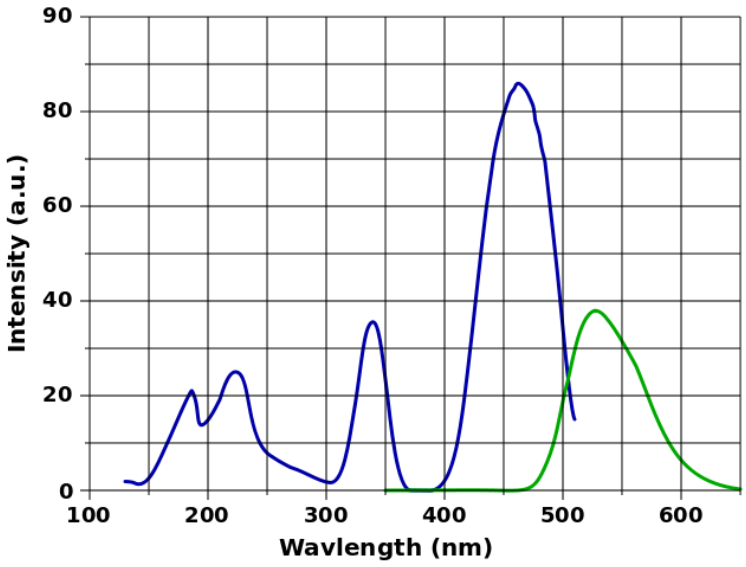

Figure 4.3: Ce:YAG emission (green) and absorption spectrum (blue)

4.1.4 Emission Properties

Emission of the Ce:YAG crystal is centered at 550 nm with a FWHM of approximately 100 nm [28]. This emission is centered on 550 nm, which is a good match to the S-20 photocathode of the streak camera. The phosphor has a broadband emission due to the 5d to 4f transition of Ce^{3+} [29]. The energy band diagram of cerium ion is shown in Figure 4.2.

The emission spectrum of a Ce:YAG crystal is due to transitions from the 5d states to the ground state which is a doublet $^2F_{5/2}$ and $^2F_{7/2}$. This provides the double peak (540 nm and 560 nm) seen in the emission spectrum of the Ce:YAG crystal Figure 4.3 [25]. The florescence lifetime of the crystal (bottom 5d to 4f transition) is approximately 70 ns making it a fast scintillator sufficient for this project [30]. The emission of the scintillator is approximately 8 photons (550 nm) per keV [31]. With the EUV light range from 62-250 eV, the expected emission is on average 0.49-1.89 photons of 550 nm light per photon of EUV light.

4.1.5 Efficiency

The florescence efficiency of the Ce:YAG is very good at approximately 75% [32]. Some of the losses in the crystal can be attributed to lattice scattering and transition losses in the energy bands. Due to the scintillators 550 nm a match of 78% with the S-20 photocathode is possible. This allows for low intensity EUV images to be resolved by the streak camera.

4.1.6 Optical Properties

Ce:YAG is highly transmissive in the visible spectrum allowing the 550 nm light to propagate with low loss. This however is not as important to EUV due to its high absorption into all materials. Once the EUV is absorbed into the face of the crystal the visible light generated propagates through the crystal with a divergent path. This causes some of the visible light to be internally reflected due to the critical angle of the material. The refractive index at visible light wavelengths is 1.82. Using Snells law the critical angle is calculated using the following equation.

$$\sin^{-1}\left\{\frac{n_2}{n_1}\cdot \sin\theta_2\right\} = \theta_{critical}$$

where θ_2 equals 90 degrees, n_1 is the refractive index of Ce:YAG (1.82), n_2 is the refractive index of vacuum (1), and $\theta_{critical}$ is the critical angle calculated to be 33.3 degrees.

CHAPTER 5: CONSTRUCTION

5.1 STREAK CAMERA

The streak camera is the core of this project and therefore all other parts of the project are built around it. The streak camera provided by Kentech was physically modified to connect to the other components such as the CCD camera and the spectrometer.

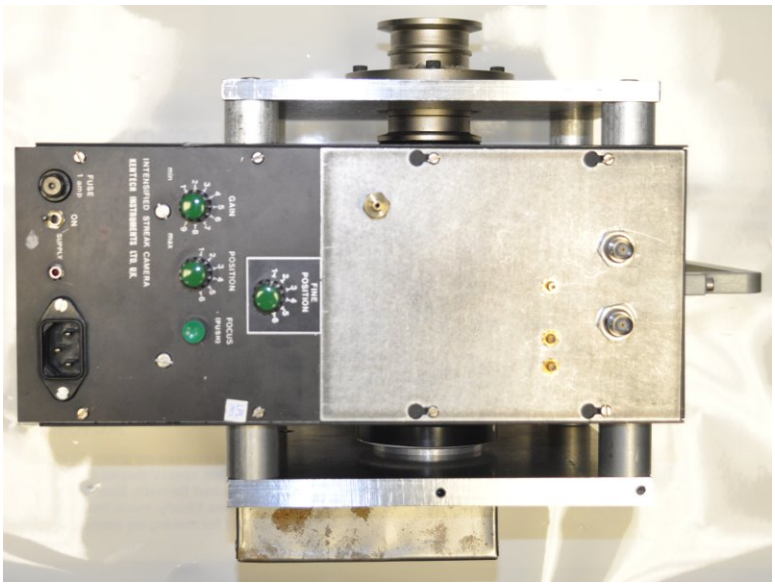

Figure 5.1: Modified streak camera showing CCD mount and spectrometer mount

The image tube of the streak camera was manufactured to have an optical path 8.5 inches above the optical table. This is too high for many optical setups, and to compensate for that the camera was rotated 90 degrees, reducing the optical path to 5 inches. To be able to rotate the camera 90 degrees, new side panels where milled out of aluminum. The connectors and adjustment knobs where moved to the top of the streak camera, as seen above in Figure 5.1. Due to the signal

propagation time in different cable lengths to the connectors the timing of the camera was re-calibrated to maintain its timings. The streak camera was manufactured with 4 1/4-20 tread mounting holes 5 inches from the optical axis of the streak camera. The holes where used to anchor the CCD and the spectrometer mounting bracket (Figure 5.1). The last modification to the SC was to replace the old bottom mount with a lightweight panel, and to machine and install a new mounting plate to the camera.

5.2 CCD

5.2.1 Preparation

In order to couple the PixeLINK PL-A741 to the streak camera several modifications had to be made. The camera has a board level CCD that is recessed into a ceramic package with a protective window. The ceramic package and the protective window interfere with coupling the CCD directly to the streak cameras output fiber plate. Conventional optics were not used due to the loss of image intensity. Therefore a coherent fiber optic taper was used.

5.2.1.1 Protective Window Removal

The protective window of the CCD in the Pl-A741 is affixed with a low temperature sealant to the ceramic package. Removal of this window was done by heating the sealant with a heat source and then prying off the window. The sealant in the window was heated to 200 ℃ for 30 second to soften the sealant. In order to heat the sealant evenly and to prevent thermal stress

in the glass, a 1/16 inch thick copper plate was cut to match the dimensions of the window and affixed to the glass with a thin layer of thermal paste. This was then placed, copper side down, on a hot plate and heated to 200 ℃ for 30 seconds or until the sealant has softened enough for the glass to be pried off. When the sealant had melted, the glass was pried off leaving the CCD and micro wires exposed. At this point a piece of cellophane tape was used to temporarily hold the protective window in place to protect it from dust and damage. [33]

5.2.1.2 Cleaning

The process of removing the protective window from the CCD caused microscopic pieces of glass fragments and sealant to fall onto the CCD surface, as seen in Figure 5.2. This debris was removed to prevent damage to the CCD and prevent degraded imaging. These particles were removed with a process known as AMD.

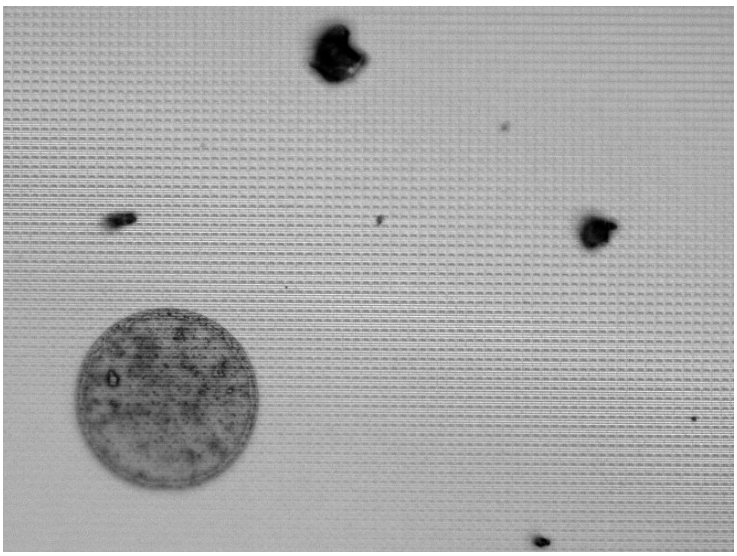

Figure 5.2: Debris on the CCD

This process is done by flushing acetone, methanol, and deionized water respectively, followed by a laminar nitrogen blow. The acetone and methanol dissolve any materials holding the particles to the CCD and the deionized water flushes any remaining particles from the surface. The nitrogen blow evaporates the water without creating turbulence that could disturb the electrical wire bonds. The AMD process was performed in a clean room and was repeated until the surface of the CCD was sufficiently clean. Upon the final AMD the CCD was sealed with a piece of cellophane tape to protect it and to keep out particles until the taper is mounted.

5.2.1.3 Optical Taper Mounting

The fiber optic taper was made of a fused bundle of 6 µm multi-mode fibers, 18 mm in diameter, which was tapered to 2/3 of an inch, and chamfered to match the profile of a 2/3 inch CCD. This taper reduces the image by 1.3 to the CCD allowing each pixel in the CCD to capture more light from the streak camera and to increase the surface area that the CCD images.

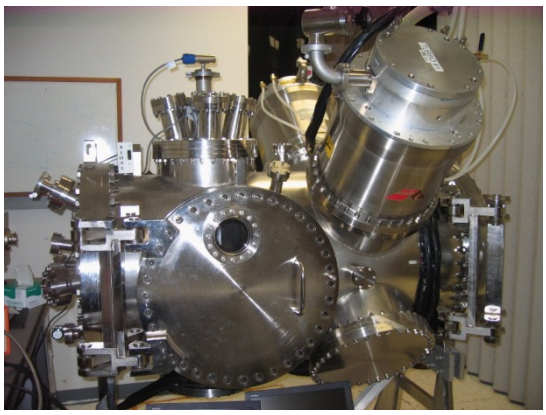

Figure 5.3: Vacuum chamber used to remove air pockets in the epoxy

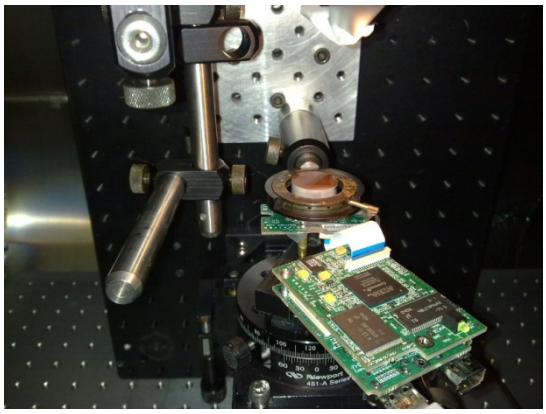

Figure 5.4: Mounting jig with taper in final position

In order to mount the taper to the CCD an index matching epoxy with low cure shrinkage was used to prevent movement of the taper and to optically couple the taper to the CCD. The epoxy used was Norland Optical adhesive 61, which provides low shrinkage and an optical index of 1.56 which is close to that of the taper. A jig was made for gluing to hold the taper precisely with respect to the CCD, and was installed in a vacuum chamber as seen in Figure 5.3. The jig provided six axis of motion to adjust the taper to a precise position and to make it parallel to the CCD. Epoxy was applied to the CCD while it was connected to a computer to provide a visual reference of the positioning of the taper. The taper was lowered into position with a light source shining through the taper. The image of the taper recorded by the CCD became sharper, as distance between the taper and CCD approached contact, providing an indicator of the position of the taper. Once the taper was in place the taper was released from the jig to allow the weight of the taper to push out the excess epoxy, and to remove and stress in the bonding as seen below in Figure 5.4. After a rest period of 15 minutes the vacuum chamber was sealed and pumped down to 50 millitorr for 15 minute to remove any air pockets.

After returning to atmospheric pressure and a rest period of 15 minute, a UV light source was applied through the taper for 10 minute to cure the epoxy. Extra epoxy was also applied to the bonding wires to secure them from damage. The final assembly was let to sit for 1 week to provide a complete curing and bond. After curing, the CCD taper assembly was strong enough to handle.

5.2.2 Mounting/Interfacing

The CCD taper assembly needed a mount that could hold the taper in contact with the fiber faceplate on the phosphorus side of the streak camera. In addition, the mount had to support both, the CCD and taper parallel to the surface of the streak camera and allow for small adjustments of tilt of the image on the CCD. To satisfy these requirements, an aluminum mounting block was made to attach the existing CCD mounting and the attached taper securely to each other so that the stress on the glue bond was reduced. This cylindrical CCD assembly was then fitted to a mounting plate that was attached to the streak camera and had the remainder of the CCD cameras electronics mounted on it. To reduce the loss of light due to the index mismatch and Fresnel reflections a thin layer of FSI optical couplant F1-0001K was applied to the surface of the taper that contacts the streak camera. The CCD camera assembly was then pressed into the mounting plate and into contact with the faceplate of the streak camera until all the air pockets had been pushed out. Once in this position, the set screws where tighten to secure the CCD camera to the streak camera. With the CCD in place, the CCD was electrically connected to the system through a 30 pin ribbon cable (Figure 5.5), and a protective shroud was

installed to shield the electronics from electrical noise, and to protect the CCD from stray light and physical damage.

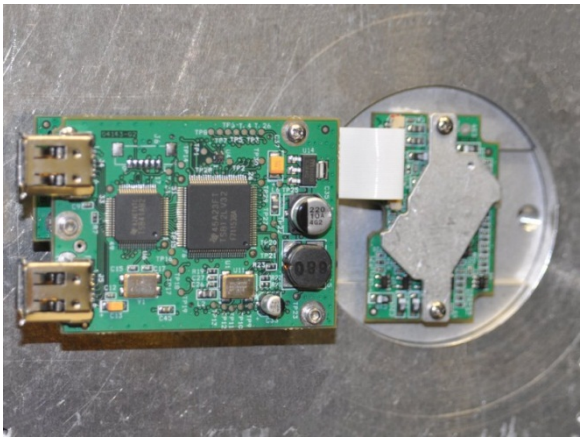

Figure 5.5: CCD mounting bracket on Streak camera

5.2.3 Electrical

The electronics in the Pl-A741 camera has 3 external connectors, one for CCD triggering and general purpose output called the machine vision connector (MVC), and two for the IEEE 1394 (Firewire) bus. The two IEEE 1394a connectors provide power to the camera and output for the captured images to the computer. Serial IEEE 1394 devices can be connected in series with the Pl-A741 using both connectors.

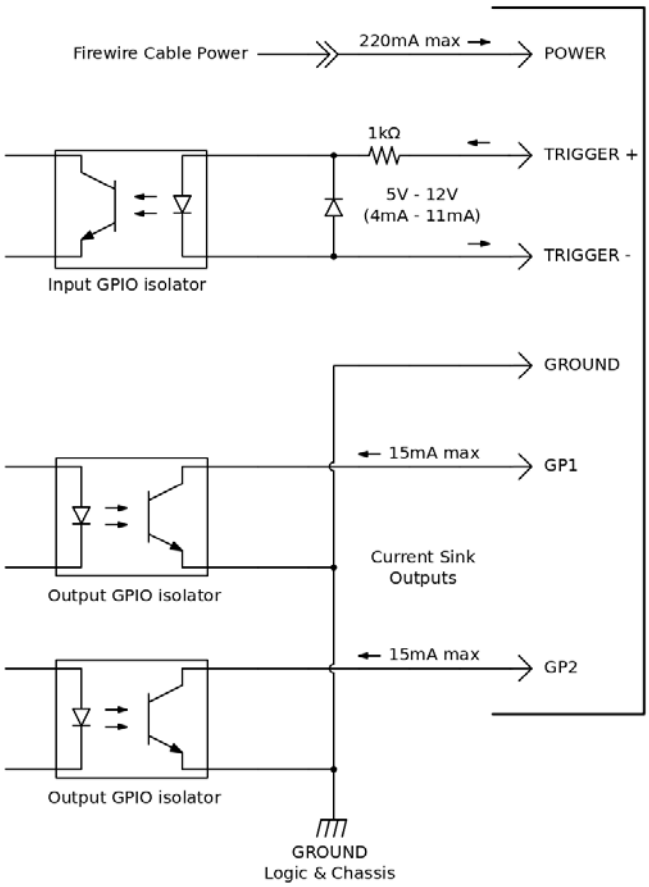

Figure 5.6: HR10A-7P-6P interface schematic [20]

The MVC (Figure 5.6) is for triggering the CCD, and for general purpose output signals sent through the IEEE1394 connectors. The control connector is a HR10A-7P-6P connector with 6 pins with their function listed below Table 5.1.

Table 5.1: Pin description of the HR10A-7P-6P connector

Pin	Name	Description
1	Power	FireWire cable power 8-30 VDC (typically 12 V) 250 mA
2	Trigger	Positive termination of optically isolated trigger input
3	Trigger-	Negative termination of optically isolated trigger input
4	Ground	Logic and chassis ground
5	GP1	General Purpose Output 1
6	GP2	General Purpose Output 2

An adapter was made to connect the MVC 2 and 3 to a female BNC connector. The positive trigger was connected to the center pin of the BNC and the negative trigger was connected to the shield of the BNC. This allowed for triggering of the CCD's optically isolated trigger through an external devise to synchronize the image capture to the streak cameras trigger.

5.3 CE:YAG SCINTILLATOR AND ZIRCONIUM FILTER

The Ce:YAG crystal was used to convert EUV light to visible light. Due to this crystal's sensitivity to wavelengths from EUV through visible, a zirconium (Zr) filter was included to filter all but the imaged EUV light. The zirconium filter is a 300 nm foil mounted on a stainless steel ring with an aperture of 1 cm

5.3.1 Mounting

In order for EUV light to be imaged by the streak camera, the Ce:YAG crystal had to be as close as possible to the input fiber optic faceplate and be contained in vacuum. The mount must also hold a 25 μm slit between the scintillator and the streak camera, and a zirconium filter to block non-EUV wavelengths. To accomplish this, an aluminum mount was made that also served as a gasket to seal the vacuum to the streak camera. This mount had a Viton O-ring around the perimeter that is in compression between the vacuum flange system and the streak camera. The mount also held the Ce:YAG against the slit on the faceplate. To balance the pressure applied by the mount on the crystal a 0.5 mm O-ring is placed between the crystal and the mount as seen in Figure 5.7.

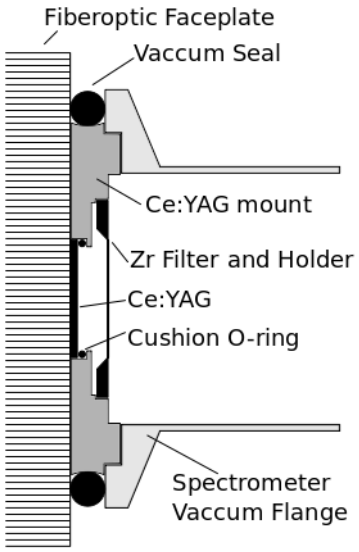

Figure 5.7: Ce:YAG and zirconium filter mount layout

The zirconium filter is mounted in close proximity (4.6 mm) to the Ce:YAG crystal to prevent non-EUV wavelengths of light from illuminating the scintillator and to reduce the possibilities of pressure gradients from forming across the filter. Due to the filters thinness and its unsupported surface, venting holes where installed to relieve any pressure gradients in the chamber from tearing the filter.

5.4 SPECTROMETER

5.4.1 Description

The spectrometer is a grazing incident flat-field spectrometer with a convex compensated variable line spacing diffraction grating. Due to this compensation the spectrometer is bound by the Rowland circle configuration (as discussed earlier), with the exception of the spectral image which is projected flat due to the compensation of the grating.

5.4.2 Mounting

Due to the absorption of EUV in air, the diffraction grating must be contained in vacuum of at least 10^{-3} torr. This was accomplished by a stainless steel vacuum flange system connected to the laser plasma chamber as seen in Figure 5.8.

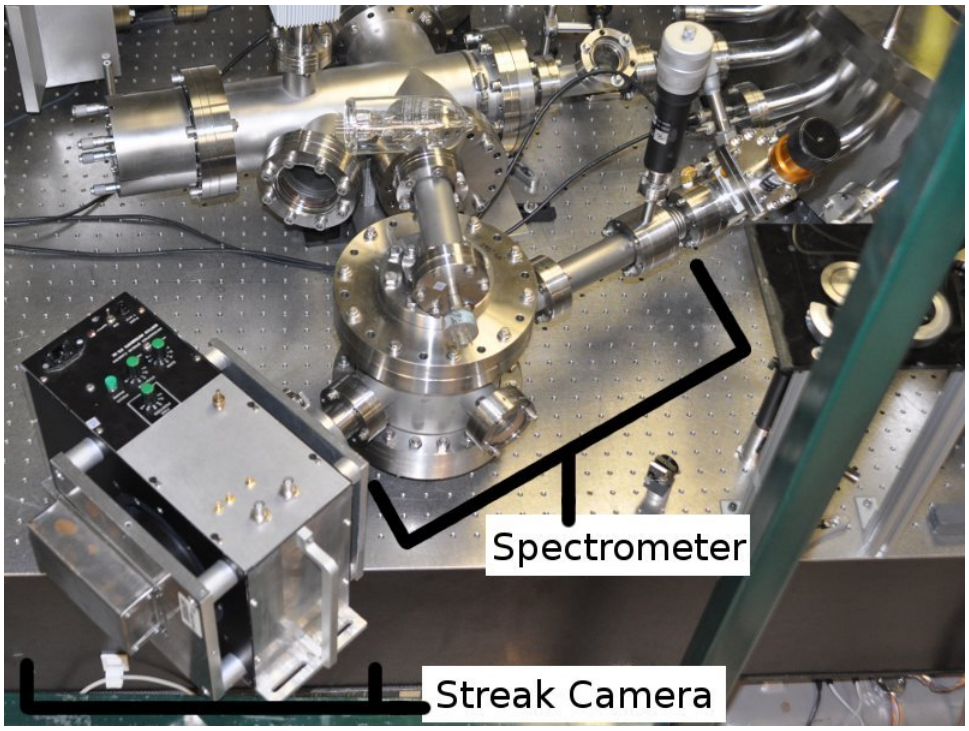

Figure 5.8: Streak camera and Spectrometer in vacuum setup for EUV imaging

The entrance slit is mounted 298 mm from the diffraction grating with a mechanical feed through to allow the aperture of the slit to be adjusted. This provides a narrow slit of light that falls on the center of the grating at a grazing incident of 87 ℃. The grating is mounted on a three-axis rotational stage that allows for alignment of the diffraction grating. Diffracted light from the grating then is transmitted to the Ce:YAG crystal, which converts the light into visible light for the streak camera. The spectrometer is coupled to the streak camera by an aluminum bracket that holds the Ce:YAG crystal and filter in place as seen in Figure 5.7

5.4.3 Alignment

Alignment of the spectrometer is critical to acquiring accurate data and necessary to select the desired wavelength to image. In order to align the spectrometer, the aperture slit and the center of the grating must be in alignment with the light source to be imaged. In this case, the light source is laser produced plasma. Due to the difficulty of aligning the spectrometer with the plasma source, a 543 nm HeNe laser was used. The laser beam was placed where the plasma would be produced and directed toward the spectrometer. The spectrometer was then positioned so that the 543 nm laser beam passed through both slits in the spectrometer and grazed across the center of the diffraction grating. The grating was rotated so that the first order diffraction of the 543 nm light falls on the wall of the 6 inch diameter vacuum chamber. In order for the desired wavelength of 5 nm-20 nm to fall within the 12.5 degree range of the output flange, the corresponding angle for the 543 nm light was calculated by using

$$m \cdot \lambda = \sigma_0(\sin\alpha + \sin\beta)$$

where m is the diffraction order, σ_0 is the nominal grove spacing, α is the incidence angle from the normal of the diffraction grating, and β is the diffraction angle with respect to the normal of the grating as seen in Figure 5.9 [14]. Once this angle was known the diffraction grating was adjusted so that the 543 nm light matched the desired angle.

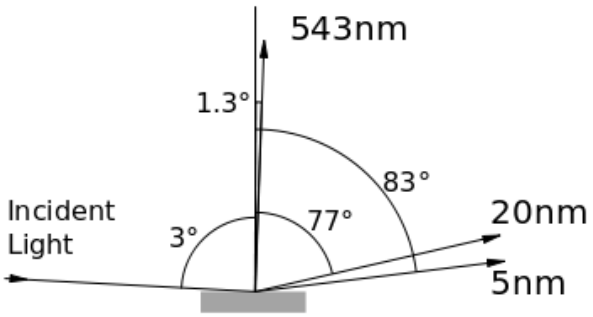

Figure 5.9: Light path angles associated with diffraction grating

With the preliminary alignment completed, the He-Ne beam was removed and the plasma chamber and the spectrometer where placed under vacuum and a laser produced plasma of water was produced. An image of the plasma was obtained using the static mode of the streak camera. The resulting image provided a spectrum which was compared with known spectrum of H_2O to show the alignment of the grating. With the known error in the pre-alignment, the pressure on the spectrometer was returned to atmosphere and the diffraction grating was adjusted to correct for the alignment. This process was repeated until the desired spectrum was shown in the streak camera.

CHAPTER 6: RESULTS

6.1 VISIBLE LIGHT IMAGING

The streak camera natively supports visible light imaging through the S-20 photocathode. Due to the spectrometer's useful range lying only within the EUV band, the spectrometer was removed from the streak camera for direct visible imaging. Visible light tests where preformed to verify the operation of the streak camera and to adjust the timings and the gain of the CCD camera and streak camera.

6.1.1 Static Imaging

Static imaging was used to measure the resolution of the streak camera and the CCD camera assembly. The light source used was an incandescent light source with a diffuser and collimating optics. This provided an even light source to illuminate a resolution chart. The resolution chart was placed in direct contact with the input fiber optic faceplate and illuminated. The camera was set to its lowest gain setting and the light source was set to a level just sufficient to have an image recorded by the CCD. The low light levels prevented saturation for the photocathode and helped resolve resolution. [18] The CCD camera was set to capture a 30 ms exposure at a gain of 9 dB. The streak camera was set into static mode by the DC voltage button to turn on the multichannel plate for continuous imaging.

The static visible light image, as seen in Figure 6.1, was processed with image processing software to obtain the maximum resolution of the system by calculating the modulation transfer function (MTF).

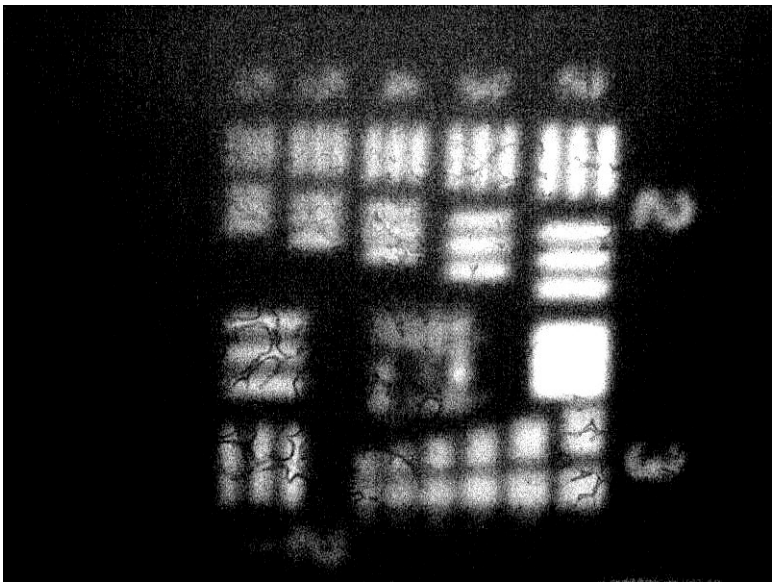

Figure 6.1: Static image of the 1951 USAF resolution chart

The resulting measured resolution was about 5.5 line pairs per mm (lp/mm) where a higher number of line pairs is s better resolution. The theoretical maximum resolution was calculated to be 248 lp/mm (vertical axis) for the CCD camera, 155 lp/mm for the taper and 101 lp/mm for the streak camera. These combine for a maximum resolution of 83 lp/mm. The discrepancy between the theoretical and measured maximum resolution is due to the interface of the input fiber optic faceplate, the scattering caused by the photocathode, scattering of the image tube, the output fiber optic faceplate, the fiber optic taper, and the CCD. The interface of these elements combine to reduce the maximum resolution of the total system due to phase noise and the multiplication of the individual component's MTF. [22]

6.1.2 Streak Imaging

With the static spatial resolution known, the temporal resolution of the camera needed to be determined. For the visible light streak imaging, a train of short laser pulses needed to be imaged by the streak camera directly. To provide the laser pulses a Ti:Sapphire 400 nm laser with a 1 kHz rep-rate and 100 fs pulse width was used. Due to the streak cameras speed, it was unable to resolve more than one pulse in one streak cycle. To provide several pulses within a 30 ns window, a multi-pass optical system was constructed (as described in chapter 2) to produce an optical delay of 4.47 ns. The camera was set to its lowest gain setting and the CCD was set to 9 dB. A neutral density filer in the laser path was adjusted until an image could be seen in static image mode. Once a static image was obtained the camera was connected to the lasers trigger with a delay generator and an electronic pulse picker to trigger the camera on a laser pulse once every second. The delay generator triggered the MCP 90 ns, and the sweep trigger 42 ns before the laser pulse reached the photocathode. The CCD camera was configured to trigger when the light reached the photocathode and integrate for 99.5 ms. Figure 6.2 was captured with the camera running at a 1Hz repetition rate.

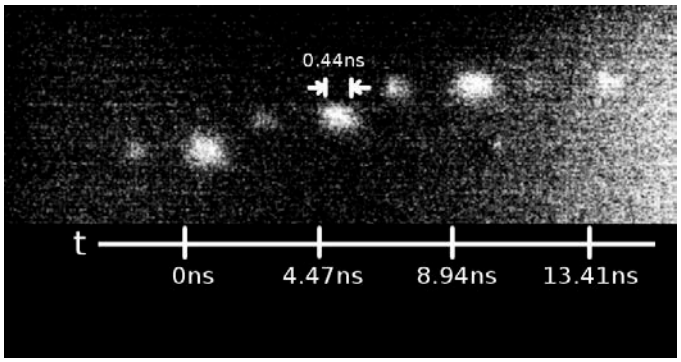

Figure 6.2: Streak image of 4 200 fs pulses

To determine the temporal resolution the distance between pulses in the image was measured. This provided a known time per distance value that was then used to calculate the time of the pulse width. Due to the short pulses (100 fs) of the laser being shorter than the measured FWHM of 440 ps in Figure 6.2, it can be deduced that the pulse width is due to the decay time of the photocathode. The decay time limits the maximum temporal resolution of the system to 440 ps. The temporal width of the streak image was calculated to be 31 ns. A 50 ps jitter was observed in between several images. This was later determined to be caused by improper trigger voltage levels (4 V) and the accuracy of the pulse picker. This error did not impact the temporal resolution measurements, as the jitter only caused a shift of the pulses by the corresponding 50 ps distance in the image. This was later remedied by a higher voltage (10 V) delay generator and eliminating the electronic pulse picker and triggering the laser every 1 second.

6.2 EUV IMAGING

For EUV imaging tests the Ce:YAG scintillator and zirconium filter where added to the streak camera to convert the EUV light to visible light that the streak camera can resolve. For the static imaging, a 40 μm slit was added without the spectrometer to determine the capabilities of the Ce:YAG and the camera to image EUV light.

6.2.1 Static EUV Imaging

To determine the resolving power of the system to image EUV, the camera was connected to a vacuum chamber with the Ce:YAG and zirconium (Zr) filter. The EUV laser plasma discussed earlier was pumped with an Nd:YAG laser to produce plasma at a repetition rate of 100 Hz. In order for EUV to propagate to the camera with minimal loss, the chamber, Zr filter, and Ce:YAG scintillator was maintained in a vacuum of 10^{-4} torr. [6] This produces the spectrum of EUV light as seen in Figure 6.3. This light is filtered by a 3 μm Zr filter to prevent other wavelengths of light from illuminating the Ce:YAG crystal. The transmission of the Zr filter in the EUV band was determined by the Center for Research in X-ray Optics [34]. This spectra multiplied together with the EUV spectra (Figure 6.3a) provided the spectrum of light incident on the Ce:YAG crystal as shown in Figure 6.3b.

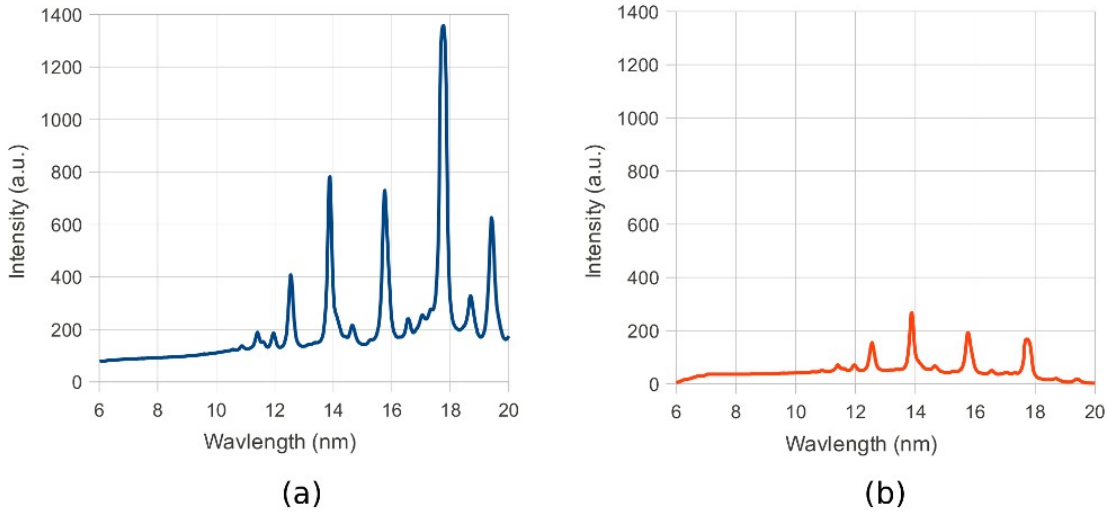

Figure 6.3: EUV spectrum from 5-20 nm without filter (a), and with zirconium filter (b)

The 40 μm slit was placed at 830 mm from the plasma and the camera was placed 40 mm from the slit for a total of 870 mm from plasma to Ce:YAG. This distance was to simulate the distance included with the installation of the spectrometer. Due to the losses involved with filtering the EUV, the limited intensity of the pump laser, and the distance involved, the gain on the streak camera need to be increased to compensate. The streak camera was set to its second gain setting and the EUV source was adjusted to its brightest setting to have an image resolvable by the CCD camera. The CCD camera was set to capture a 1 second exposure (100 pulses) and a gain to 11 dB. The streak camera was set into static mode by the DC voltage button to turn on the multichannel plate for continuous imaging. The resulting image (Figure 6.4) was captured showing the line of the EUV caused by the 40 μm slit. The line in the image is calculated to be 390 μm thick in the vertical dimension. This is due to diffraction and divergence of the EUV through the slit, as well as to visible light scattering in the Ce:YAG scintillator.

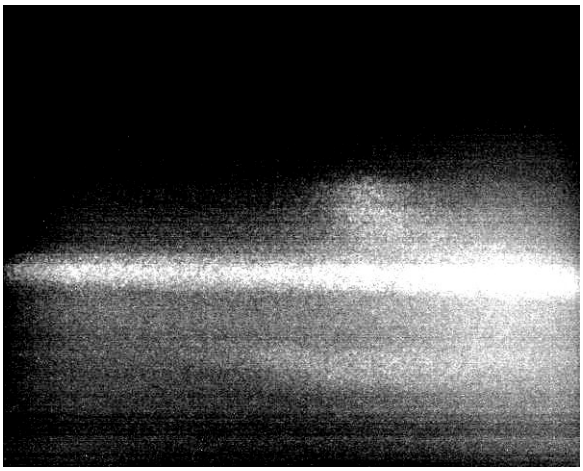

Figure 6.4: Static image of 390 μm EUV projection through 40 μm slit

6.2.2 Streak Imaging

To verify that the EUV camera was able to resolve an EUV streak the streak camera needed to capture one event plasma event with a variation in intensity. The pump laser was a Nd:YAG laser with an 8 ns pulse width. However, the EUV light pulse varied depending on the timing of the droplet with the laser and the formation of the plasma. In order to properly test the streak camera the sweep trigger had to be synchronized with the leading or falling edge of the laser produced plasma. The Q-switch of the EUV pump laser was used to trigger the delay generator with a 1 Hz pulse rate. The camera was set to its second gain setting and the CCD camera was set to 12 dB. The delay generator triggered the MCP 90 ns, and the sweep trigger 42 ns before the EUV pulse reached the photocathode. The CCD camera was configured to trigger when the light reached the photocathode and integrate for 99.5 ms.

CHAPTER 7: CONLUTION

The EUV streak camera using Ce:YAG was proven successful for imaging EUV and for providing 440 ps resolution streaked images. This system provides a robust solution for imaging spectral data for the EUV band over short periods of time. Due to losses in the diffraction grating and the intensity of the EUV source the spectral part of the camera was unable to be verified, but a brighter source, a more efficient grating, and a thinner Zr filter will improve the intensity of the image and therefore, allow for a spectral streaked image. The limiting factor in the images captured by the EUV streak camera was that size of the Ce:YAG crystal. A thinner Ce:YAG crystal will allow for less scattering and a better image coupling between the input surfaces of the Ce:YAG and the streak camera. In addition a larger diameter crystal would allow for the EUV image to be spread over a larger area of the streak camera's photocathode preventing the image from being lost to the resolution of the system.

7.1 FUTURE WORK

In the near future further improvements to the EUV spectral streak camera will be performed. The alignment of the spectrometer will allow the spectrum of the mass limited tin doped laser plasma source to be recorded for one laser pulse. With the mass and composition already known, the conversion efficiency of the plasma source can be determined. Another experiment in the near future will be the comparison of the streak camera with a calibrated "flying circus" EUV intensity meter. This meter will allow a photon budget to be determined for

the streak camera, and can be used to calculate the number of photons produced by the plasma. This will also allow for the calibration of the EUV spectral streak camera to be used as a laboratory instrument for tuning laser plasma sources.

LIST OF REFERENCES

[1] David Attwood, *Soft X-Rays and Extream Ultraviolet Radiation: Principes and Aplications*.: Cambridge University Press, 1999.

[2] Martin Richardson, , Banqiu Wu and Ajay Kumar, Eds.: The McGraw-Hill Companies, Inc., 2009, ch. Chapter 3: EUV Sources.

[3] Paul Ants Jaanimagi, "X-ray Streak Camera," University of Waterloo, University of Central Florida, Orlando, PhD Thesis 1981.

[4] Moza Al-Rabban et al., , Vivek Bakshi, Ed.: The Society of Photo-Optical Instrumentation Engineers, 2006, ch. Chapter 10: Modeling LPP Sources.

[5] J. P. Delaboudinière, G. E. Artzner, J. Brunaud, and others, "EIT: Extreme-ultraviolet Imaging Telescope for the SOHO mission," *Solar Physics*, vol. 162, pp. 291-312, 2004.

[6] Reuvani D. Kamtaprasad, "Laser Plasma Radiation Studies for Droplet Sources," University of Central Florida, Orlando, MS Thesis 2010.

[7] T. Ejima, F. Ishida, H. Murata, M. Toyoda, and others, "High throughput and wide field of view EUV microscope for blur-free one-shot imaging of living organisms," *Optics Express*, vol. 18, no. 7, pp. 7203-7209, 2010.

[8] M. Richardson et al., , Vivek Bakshi, Ed.: The Society of Photo-Optical Instrumentation Engineers, 2006, ch. Chapter 26: Laser Plasma EUV Sources Based on Droplet Target Technology.

[9] Princeton Instruments, "PIXIS-XO: 512B,".

[10] S. Xia, F. Sarubi, R. Naulaerts, S. Nihtianov, and L. Nanver, "Response Time of Silicon Photodiodes for DUV/EUV Radiation," , 2008.

[11] W. A. Soer, P. Gawlitza, M. M. J., M. J. J., and others, "Extreme ultraviolet multilayer mirror with near-zero IR reflectance," *Optics Letters*, vol. 34, no. 23, 2009.

[12] C. Montcalmand, S. Bajt, P. B. Mirkarimi, and others, "Multilayer reflective coatings for extreme-ultraviolet lithography," *SPIE*, vol. 3331, 1998.

[13] L. Poletto, G. Tondello, and P. Villoresi, "Optical design of a spectrometer-monochromator for the extreme-ultraviolet and soft-x-ray emission of high-order harmonics," *Applied Optics*, 2003.

[14] Toshiaki Kita, Tatsuo Harada, N. Nakano, and H. Kuroda, "Mechanically ruled aberration-corrected concave gratings for a flat-field grazing-incidence spectrograph," *Applied Optics*, vol. 25, p. 4228, 1986.

[15] Christopher Palmer, *Diffraction Grating Handbook*.: Newport Corporation, 2005.

[16] Inc. Hitachi High. (2009, November) Hitachi Aberration-Corrected Concave Gratings for Flat-Field Spectrographs. [Online]. http://www.lambda-at.com/pdf/ConcaveGrating-Spectrograph-Normal(1)%5B1%5D.pdf

[17] Illes P. Csorba, *Image Tubes*.: Howeard W.Sams and Co., Inc., 1985.

[18] Ltd Kentech Instruments, Operations Manual for Compact Optical Streak Camera, OSC12/25XX, 1990.

[19] B. P. Varma and C. Ghosh, "Some optical properties of a multialkali (S20) photocathode and the processng parameters," *Journal of Physics D: Applied Physics*, vol. 6, 1973.

[20] Photek Ltd. (2009, November) Photek Ltd - Photocahode Spectral Responce Curves. [Online]. http://www.photek.com/support/ti_pc_response.htm

[21] PixeLINK. (2009, November) PL-A741 Machine Vision Camera System Guide Version 4.0. [Online]. http://ftp.elvitec.fr/PixeLINK/MANUELS/PL-A741%20Manuel.pdf

[22] Glenn D. Boreman, *Modulation transfer function in optical and electro-optical systems*.: SPIE Press, 2001.

[23] MTI Corporation. (2009, Nov) Ce:YAG substrate (111) 5 x 5 x 0.5 mm, 2sp. [Online]. http://www.mtixtl.com/browseproducts/Ce-YAG-substrate--%28111%29--5-x-5-x-0.5-mm--2sp.HTML

[24] MTI Corporation. (2010, June) Czochralski Process. [Online]. www.mtixtl.com/xtlflyers/Czochralski.doc

[25] Y. Dong, G. Zhou, J. Xua, and others, "Luminescence Studies of Ce:YAG Using Vacuum Ultraviolet Synchrotron Radiation," *Materials Research Bulletin*, vol. 41, no. 10, 2006.

[26] Xinbo Yang, Hongjun Li, Qunyu Bi, and Others, "Growth of large-sized Ce:Y3Al5O12 (Ce:YAG) scintillation crystal by the temperature gradient technique (TGT)," *Journal of Crystal Growth*, no. 331, 2009.

[27] P. Schauer and R. Autrata, Optimization of scintillation detector for SEM, 2004.

[28] W. Hollerman, Stephen W. Allison, Shawn M, and others, "Comparison of Fluorescence Properties for Single Crystal and Polycrystalline YAG:Ce," in *IEEE*, 2002.

[29] S. Nishiura, S. Tanabe, K. Fujioka, and others, "Preparation and Optical Properties of Transparent Ce:YAG Ceramics for High Power White LED," *IOP Conference Series: Materials Science and Engineering*, vol. 1, 2009.

[30] D. S. Hamilton, S. K. Gayen, G. J. Pogatshnik, and others, "Optical-Absorption and Photoionization Measurments From The Excited States of Ce3+:Y5Al5012," *Physics Review B, Condensed Matter*, vol. 39, no. 13, 1989.

[31] Saint-Gobain Crystals. (2010, June) Yttrium Aluminum Garnet doped with Cerium. [Online]. http://www.detectors.saint-gobain.com/uploadedFiles/SGdetectors/Documents/Product_Data_Sheets/YAG-Data-Sheet.pdf

[32] Z. Liu, S. Liu, and K. Wang, "Measurement and Numerical Studies of Optical Properties of YAG:Ce Phosphor for White Light-Emitting Diode Packaging," *Applied Optics*, vol. 49, no. 2, 2010.

[33] R.G. van Silfhout and A.S. Kachatkou, "Fibre-optic coupling to high-resolution CCD and CMOS image sensors," School of Electrical and Electronic Engineering, The University of Manchester, 2008.

[34] Eric Gullikson. (2010, November) X-Ray Interactions With Matter: Filter Transmission. [Online]. http://henke.lbl.gov/optical_constants/filter2.html

[35] Xie Xin-Hua, Liu Ya-Qing, Fan Pin-Zhong, and Li Ru-Xin, "Spectral Focusing Characteristics of a Grazing-Incidence Flat-Field Grating Spectrometer," *Chinese Physics*, vol. 13, no. 11, 2004.

[36] Orazio Svelto, *Principals of Lasers*.: Springer Science+Business Media, Inc., 1998.

[37] Shott Fier Optics, STD 18mm TPR RD/RECT 2/3 CCD FORMAT 25728.pdf, 1997.

[38] Clarisse Mazuir, In-band high-resolution imaging of the microscopic 13nm laser plasma sources, 2004.

[39] Yu. S. Kasyanov, A. A. Malyutin, M. C. Richardson, and V.K. Chevokin, *High Speed Photography, Proceedings of the 11th Internationl Congress of High Speed Protography*.: Chapman and Hall Ltd, 1975.

[40] A. J. Alcock, M. C. Richardson, and M. Ya. Schelev, *Proceedings of the 9th Internationl Congress of High-Speed Protography*.: Society of Motion Picture and Television Engineers, 1970.

[41] Paul Ants Jaanimagi, "Ultra-Fast Infarared Diagnostics," University of Waterloo, MS Thesis 1977.